Photophysics of Organometallics

Bearbeitet von
Alistair J. Lees

Weitere Fachgebiete > Chemie, Biowissenschaften, Agrarwissenschaften > Analytische Chemie > Organometallchemie

Zu Inhaltsverzeichnis

schnell und portofrei erhältlich bei

beck-shop.de
DIE FACHBUCHHANDLUNG

Photophysics and Photochemistry of Organometallic Rhenium Diimine Complexes

Arvind Kumar, Shih-Sheng Sun, and Alistair J. Lees

Abstract This review describes the photophysics and photochemistry of various diimine rhenium(I) tricarbonyl complexes. The exceptionally diverse photophysical behavior of these complexes is largely dependent on the nature of their lowest excited states. These excited states and the excited-state characteristics can be easily changed by varying the substituents on either the diimine ligands or the ancillary ligands. The prolificacy of the photophysical and photochemical properties of diimine rhenium(I) tricarbonyl complexes allows for a range of important applications such as light-emitting devices, sensors, probes for photo-polymerization, optical switches, nonlinear optical materials, radiopharmaceuticals, carbon dioxide reduction and supramolecular chemistry. We have covered the studies that best characterize the state of the field as far as the most significant fundamental photochemical advances, and the applications of the photochemistry of rhenium complexes.

Contents

A. Kumar and S.-S. Sun (✉)
Institute of Chemistry, Academia Sinica, 128 Academia Road, Section 2, Nankang,
Taipei, 115, Taiwan, ROC
e-mail: sssun@chem.sinica.edu.tw

A.J. Lees (✉)
Department of Chemistry, State University of New York at Binghamton,
Binghamton, NY, 13902-6016, USA
e-mail: alees@binghamton.edu

1   Introduction and Scope

Photophysical and photochemical phenomena are quintessential to the survival of life on our planet. The vital role played by light in biological and materials science needs no further emphasis as the value of solar energy has never been more evident than now. The recent interest in the photophysics and photochemistry of molecules with relatively long-lived highly excited electronic states has been prompted by advances in optoelectronics and by the development of molecular logic devices [1, 2]. Photochemically stable molecules with relatively long-lived fluorescent states could act as excitation wavelength-sensitive electron or electronic energy donors/acceptors when incorporated into larger supramolecular or polymeric systems [3, 4]. The potential value of incorporating such species into molecular devices increases with their increased stability and excited-state lifetime.

Organometallic rhenium complexes occupy a prominent position in the photophysics and photochemistry of transition-metal complexes. Since the first systematic studies of the photophysical and photochemical properties of the remarkably stable complexes, fac-Re^{I}X(CO)$_3$(L) (where L is a bidentate–diimine ligand or two monodentate pyridyl ligands, and X is a halogen, an alkyl group, or a pyridyl ligand), in the 1970s by Wrighton and coworkers, polypyridyl complexes of rhenium(I) have played an important role in contributing to an understanding of the photophysical and light-induced electron-transfer (ET) and electronic energy-transfer (ENT) processes [5–9]. A number of investigations have appeared in the literature, based on complexes incorporating the Re^{I}X(CO)$_3$(bpy) chromophore (bpy = 2,2′-bipyridine or its derivatives). These have elegantly demonstrated medium effects [10, 11], fundamental photophysical properties of *metal-to-ligand charge transfer* (MLCT) excited states [12, 13], and physical and/or chemical processes facilitated by covalently linked chromophore-quencher systems [14, 15]. The rhenium(I)-based compounds offer several advantages for elucidating the various excited-state properties of organometallic complexes. As pointed out by Vogler and Kunkley, the photophysics and photochemistry of rhenium complexes is rich, spanning eight oxidation states from formal rhenium(0) (for example, Re$_2$(CO)$_{10}$) to formal rhenium(VII) (for example MeReO$_3$) [13].

The convenient and easy synthesis of fac–Re^I(CO)$_3$(diimine) complexes and the modification of the diimine ligands themselves makes systematic tuning of the

electronic properties easier for these complexes [16–18]. Altering the excited-state properties provides insight into the role of the acceptor diimine ligand in determining spectroscopic and photophysical features. Moreover, the lifetimes of the lowest excited states in these fac–$Re^I(CO)_3$(diimine)-based complexes are usually sufficiently long enough to permit energy- or electron-transfer processes to nearby components when suitable energetic and electronic conditions are satisfied [14].

In general, the excited-state properties of diimine rhenium(I) tricarbonyl complexes primarily occur through their lowest triplet excited states, due to rapid vibrational relaxation and intersystem crossing from the upper vibrational energy levels [6, 7]. Thus, the nature of the lowest-energy-acceptor ligands (either diimine ligands or bridging ligands) plays a decisive role in determining the ultimate photophysical and/or photochemical properties. Various excited states are generated, depending on the relative energy levels of the metal and ligand orbitals, as well as the extent of interaction between them. Many mononuclear diimine rhenium(I) tricarbonyl complexes are highly emissive (Φ_{em} = 0.001–0.1) and feature relatively long emission lifetimes (10 ns to 1 µs) in solution, due to the existence of lowest energy triplet-centered MLCT excited states [6, 19]. In these cases, the decay of the lowest-lying MLCT-emitting states is often primarily determined by an energy gap law effect [20]. Another prominent feature of these complexes is the large hypsochromic shift of their emission maxima on going from a fluid environment to a rigid medium and this is described as "*luminescence rigidochromism.*" Here, the long-lived triplet MLCT excited state is apparently raised in energy compared to the ground-state molecule, due to the restricted ability of the solvent molecules to reorient and stabilize the excited-state dipole moment [5, 10, 12].

Understandably, there is an enormous richness in the photophysical and photochemical behavior of the excited states present in diimine rhenium(I) tricarbonyl complexes. Indeed, this plethora of molecular photophysical characteristics has led to a wide range of interesting and important applications, including their use as catalysts [21–25], sensors [26–33], probes for photo-polymerization [10, 34, 35], optical switches [36–45], light-emitting materials [46–52], nonlinear optical materials [53–56], binding or photocleavage of DNA [57–61], and radiopharmaceuticals [62–66]. Under the purview of this article our focus will be to cover photophysical and photochemical properties and hence other aspects, such as synthetic, catalytic, pharmaceutical, etc., will not be discussed.

2 Photophysical Properties of Rhenium Carbonyl Diimine Complexes

Several transitions are possible in diimine rhenium(I) tricarbonyl complexes, such as *ligand field* (LF), *metal-to-ligand charge transfer*, *ligand-to-ligand charge transfer* (LLCT), *σ-bond-to-ligand charge transfer* ($\sigma \rightarrow \pi^*$), and *intraligand* (IL) excited states. Recently, density functional theory (DFT) and time-dependent density functional theory (TD-DFT) have provided new insights into the appropriateness of

these models [67–73]. For the "parent complexes," [Re(bpy)(CO)$_3$Cl] and [Re(bpy)(CO)$_3$(py)]$^+$, the *highest occupied molecular orbital* (HOMO) contained 50% or greater Re$_d$ character along with ~20% contributions each from CO and Cl for [Re(bpy)(CO)$_3$Cl] and ~20% contributions from CO for [Re(bpy)(CO)$_3$(py)]$^+$. The *lowest unoccupied molecular orbital* (LUMO) consists of 80% or greater diimine ligand π* character in both cases. Thus, the lowest energy optical transition was assigned as *a metal-ligand-to-ligand charge transfer transition* (MLLCT) [67].

Similarly the HOMOs of [Re(diimine)(CO)$_3$(RNC)]$^+$ complexes contained 45% or greater Re$_d$ character and 27% or greater RNC character in general, where RNC is 6-dimethylphenylisocyanide and diimine is phenanthroline derivatized with electron-donor groups or electron-withdrawing groups, whereas the LUMOs contained >81% diimine π character [68, 69]. Hence, the lowest optical transition was assigned as MLLCT. The HOMOs of complexes of the type [Re(bpy)(CO)$_3$(ER)$_2$], where ER = NHPh, N(4-CH$_3$Ph), PPh$_3$, were located on the amido and phosphido ligands and the LUMOs were located on the π(bpy) levels. Thus, the lowest energy transition was assigned as LLCT and emission as ^{3}LLCT for these complexes [70].

2.1   Complexes with Lowest MLCT Excited States

The MLCT absorption band of the rhenium carbonyl complexes often lies at lower energy on the shoulder of the π–π* diimine *ligand-centered* transition (LC); hence, both the ^{1}MLCT and ^{1}LC levels are often populated simultaneously. Further, the ^{3}MLCT and ^{3}LC vary in energy relative to one another. Consequently, emission spectra are often found to occur in the 500 nm region with strong vibronic character consistent with a large ^{3}LC contribution; in other cases the spectra occur near 600 nm which are structureless and assignable to a ^{3}MLCT state. However, as the emission envelope of the coordinated diimine ligand is red-shifted from that of the free ligand, a combination of ^{3}LC and ^{3}MLCT states is often employed to account for the emission behavior (see Fig. 1).

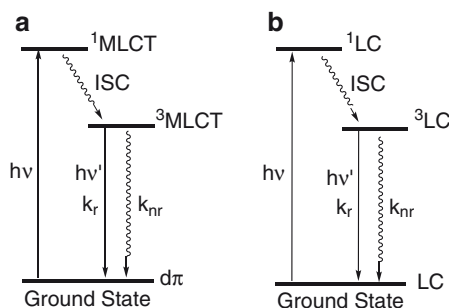**Fig. 1**   Jablonski diagram for [Re(diimine)(CO)$_3$L] complexes: (**a**) MLCT model, (**b**) ligand-centered model. The k_r and k_{nr} are the radiative and nonradiative decay constants from the excited state to the ground state

These bands show negative *solvatochromism* as revealed by band shifts to lower energy in less polar solvents [5, 7, 8, 12]. The direction of the solvent dependence is associated with a reduced (and reversed) molecular dipole in their MLCT excited states. Emissions from these complexes are typically broad and structureless, and they also often exhibit a *rigidochromic effect* [7–12]. Tables 1 and 2 summarize the luminescence characteristics and environmental effects on absorption and emission maxima for rhenium(I) tricarbonyl diimine complexes.

Both the emission quantum yields and lifetimes are significantly increased on cooling the solution to 77 K, implying that the radiative decay pathways are favored in the more rigid environment; the emission lifetimes are typically governed by the *energy gap law* [17, 20, 74, 75]. Table 3 summarizes the excited-state decay parameters for the MLCT excited states of *fac*–[ClRe^I(4, 4′–(X)$_2$–bpy)(CO)$_3$] complexes (where 4,4′–(X)$_2$-bpy is 4,4′-disubstituted-2,2′-bipyridine).

These complexes also usually exhibit substantial photostability under visible light irradiation and, due to their relatively long-lived triplet excited-state characteristics, the emission lifetimes are easily quenched by bimolecular electron- and/or energy-transfer processes in solution [6, 76]. The electronic structures of MLCT excited molecules of diimine rhenium(I) tricarbonyl complexes can be viewed as a charge-separated species, [LRe^{II}(CO)$_3$(diimine$^{•-}$)]*, with an essentially oxidized

Table 1 Luminescence characteristics for various [LRe(CNx)(CO)$_3$](PF$_6$) complexes (CNx = 2, 6-dimethylphenylisocyanide) in EtOH:MeOH (4:1, v/v) (data taken from [68])

L	λ_{em} (10^3 cm^{-1})		τ_{em}(μs)	τ_{em}(μs)	Φ_{em}
	77 K	298 K	77 K	298 K	298 K
1,10-Phenanthroline	21.8	19.7	65	8.6	0.77
	20.4				
	19.1				
	17.7				
5-Chloro-1,10-phenanthroline	21.1	19.1	171	1.5	0.78
	19.7				
	18.3				
	17.1				
5-Nitro-1,10-phenanthroline	20.4		322		
	19.0				
	17.8				
5-Methyl-1,10-phenanthroline	21.6	19.6	231	20.2	0.83
	19.3				
	18.8				
	17.5				
5,6-Dimethyl-1,10-phenanthroline	20.7	20.3	229	30.9	0.56
	20.4	19.3			
	18.0				
	16.6				
1,10-Phenanthrolinopyrrole	20.4	18.5	268	6.2	0.11
	18.6				
	17.3				
	16.0				

Table 2 Environmental effects on absorption and emission maxima of [ClRe(CO)$_3$L] (data taken from [6])

L	Environment (T, K)	First λ_{abs} (10^3 cm^{-1})	λ_{em} (10^3 cm^{-1}) (Φ_{em}, ±15%)	τ (µs)
Phen	CH$_2$Cl$_2$ (298)	26.3	17.33 (0.36)	0.3
	Polyester resin (298)		18.52	3.67
	EPA (77)		18.94 (0.33)	9.6
5-Cl–phen	CH$_2$Cl$_2$ (298)	25.91	17.12	
	Pure solid (298)		17.99	
	EPA (77)		18.69	6.25
5-Br–phen	Benzene (298)	25.32	17.15	≤0.65
	CH$_2$Cl$_2$ (298)	25.84	17.12 (0.20)	
	MeOH (298)	26.88	17.04	
	Pure solid (298)		17.83	
	Polyester resin (298)		18.32	2.2
	EPA (77)		18.69 (0.20)	7.6
5-Me–phen	Benzene (298)	25.65	17.00	≤0.65
	CH$_2$Cl$_2$ (298)	26.32	17.01 (0.30)	
	MeOH (298)	27.05	17.00	
	Pure solid (298)		18.42	
	Polyester resin (298)		18.48	3.5
	EPA (77)		18.83 (0.33)	5.0

Table 3 Excited-state decay parameters for the MLCT excited states of *fac*-[ClRe^I(4,4′-X$_2$-bpy)(CO)$_3$] in THF (data taken from [17])

X	λ_{em} (nm) 77 K	295 K	Φ_{em}	τ (µs) 77 K	τ (ns) 295 K	$10^4 k_r$, s^{-1} (295 K)	$10^6 k_{nr}$, s^{-1} (295 K)
NEt$_2$	501	575	0.033	12.5	412	7.9	2.4
NH$_2$	502	573	0.020	11.0	262	7.8	3.7
NHCOCH$_3$	535	620	0.0073	4.60	65	11.0	15.0
OCH$_3$	525	630	0.0028	3.66	26	10.0	37.0
CH$_3$	530	626	0.0057	3.45	49	12.0	20.0
H	540	642	0.0031	3.12	39	8.0	26.0
Ph	560	647	0.0084	4.36	56	15.0	18.0
Cl	580	700	0.0006	1.15	9	6.7	110.0
CO$_2$Et	598	715	0.0014	2.93	15	9.3	67.0
NO$_2$	670	780	<0.0001	0.86	<6	1.7	167.0

metal center and reduced diimine ligand. The MLCT excited state experiences a decrease in the extent of Re-CO π-back bonding, and this effect can be easily monitored by time-resolved IR spectroscopy and time-resolved resonance Raman spectroscopy [77, 78]. Indeed, the nanosecond time-resolved IR spectrum of ClRe(CO)$_3$(bpy) shows an average shift to higher energy by 55 cm^{-1} in the three ν(CO) bands and the transient infrared spectrum of [(4-Me-py)Re(phen)(CO)$_3$)]$^+$ shows an average shift to higher energy by 46 cm^{-1} in the three ν(CO) bands [79, 80]. Thus, time-resolved IR spectroscopy has been able to differentiate the lowest excited state between MLCT or IL levels in ClRe(bpy)(CO)$_3$ containing phenyle-

neethynylene oligomers [81]. Transient resonance Raman spectroscopy also provides evidence, based on the resonance enhancement of the ν(CO) Raman peaks, for identifying the lowest excited states and possible excited-state intermediates [82, 83]. In such cases, intense excited-state Raman lines have been observed that are associated with the radical anion of the diimine ligand.

2.2   Complexes with Lowest LLCT Excited States

In complexes with both reducing- and oxidizing-type ligands, excited states can arise that are the result of charge transfer from one ligand (donor) to another ligand (acceptor). Several rhenium tricarbonyl-based chromophore-quencher complexes are known to have lowest excited states featuring LLCT character [16, 84]. Owing to the very weak electronic interaction between the donor and the acceptor components, the extinction coefficients for such LLCT bands are usually very low. For example, the extinction coefficient of the LLCT band for complex $[(py–ptz)Re^I(CO)_3(bpy)]^+$ is only 2.4 M^{-1} cm^{-1} [85]. Nevertheless, the LLCT state can be indirectly populated by MLCT excitation followed by an intramolecular electron-transfer process. For example, in the case of the chromophore-quencher complex $[(py–ptz)Re^I(CO)_3(bpy)]^+$, optical excitation into the $d\pi(Re)$ to $\pi^*(bpy)$ MLCT transition generates the excited-state species, $[(py–ptz)Re^{II}(CO)_3(bpy^{•-})]^+$ [86]. Thereafter, rapid electron transfer from py-ptz to Re^{II} takes place, with a determined rate constant higher than 4.8×10^9 s^{-1}. The species subsequently formed is $[(py–PTZ^{+•})Re^I(CO)_3(bpy^{•-})]^+$, which can be considered as a py–PTZ to bpy charge transfer (LLCT) excited state (see Fig. 2). Direct evidence for the formation of this charge-separated species has been provided from time-resolved resonance Raman and absorption spectroscopies, revealing that the complex has both the characteristics of the reduced $bpy^{•-}$ and oxidized $PTZ^{+•}$ moieties [84, 87, 88]. The LLCT excited state decays to the ground state via back electron transfer from bpy to ptz with a rate constant of 1.1×10^7 s^{-1} [87]. Typically, the nonradiative decay parameters of the LLCT excited states in such complexes with similar bipyridyl derivatives follow the *energy gap law*. Figure 2 below shows the electron-transfer processes taking place in such systems.
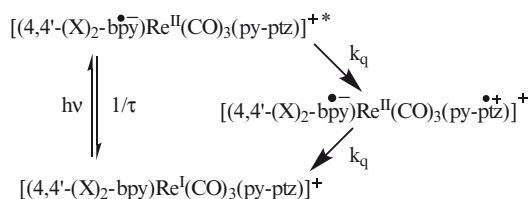

Fig. 2 Excited state dynamics of $[(py-PTZ)Re^I(CO)_3(bpy)]^+$ (reproduced with permission from [87])

In another typical case, the complex $[Re^I(MQ^+)(CO)_3(dmb)]^{2+}$, (where MQ^+ = *N*-methyl-4,4′–bipyridinium and dmb = 4,4′-dimethyl-2,2′–bipyridine) the optical excitation (400 or 355 nm) of the complex populates a Re→dmb ^{3}MLCT excited state $*[Re^{II}(MQ^+)(CO)_3(dmb^{•-})]^{2+}$. A picosecond dmb$^{•-}$→MQ$^+$ interligand electron transfer (ILET) follows, producing a Re→MQ$^+$ MLCT excited state $*[Re^{II}(MQ^•)(CO)_3(dmb)]^{2+}$. The ILET rate (8–18 ps, depending on solvent) being accelerated by a combination of large electronic coupling through Re^{II} and vibrational excitation of the ^{3}MLCT (dmb) precursor state (see Fig. 3) [89].

Because of the generally nonemissive nature of LLCT states, their excited-state properties can be studied only by transient spectroscopy, or indirectly analyzed by their effect on the MLCT excited-state lifetimes of the emissive chromophores. However, if the electron-donor ligand is not stable toward oxidation, then subsequent photochemical reactions may occur. Thus, these irreversible photochemical reactions can be monitored to quantitatively determine the photophysical parameters
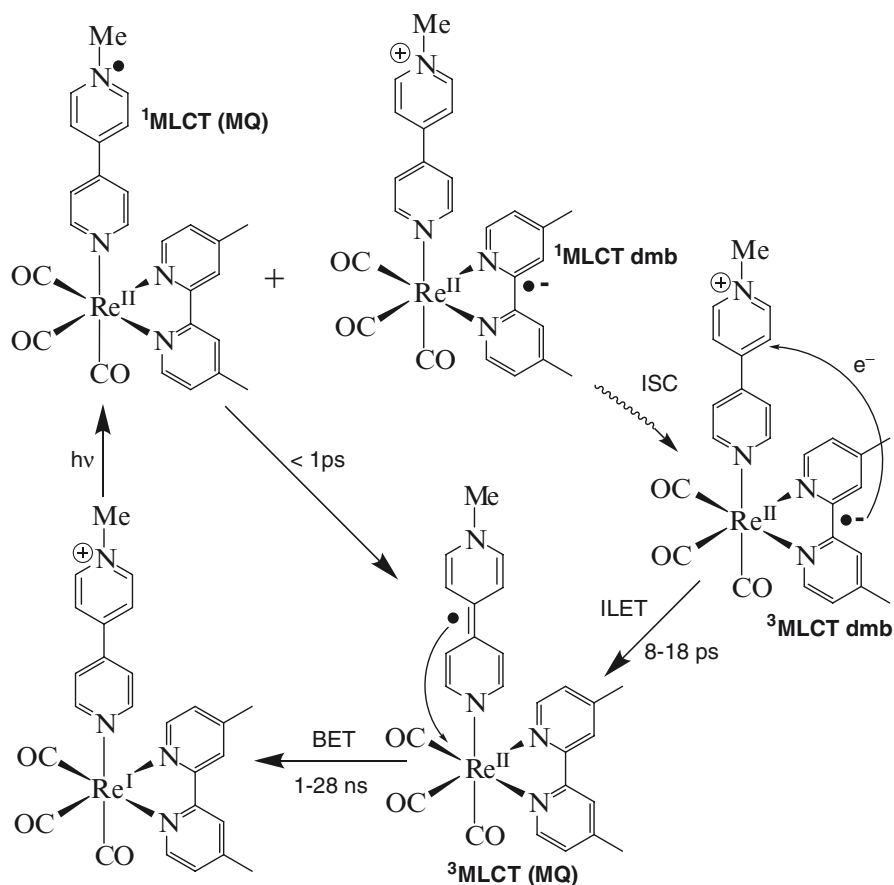

Fig. 3 Excited state dynamics of $[Re^I(MQ^+)(CO)_3(dmb)]^{2+}$ (reproduced with permission from [89])

of LLCT states [90–95]. Figure 4 depicts the excited-state processes of a typical example, involving the rhenium chromophore coordinated to a 1, 2-diamine donor ligand [95]. Initial photoexcitation produces the relaxed $d\pi(Re)\rightarrow\pi^*(bpy)$ MLCT excited state.

The MLCT state relaxes via radiative and nonradiative decays to the ground state (k_d path) or by forward intraligand electron transfer (ET) from the diimine donor to the photoexcited Re(I) center (k_{FET}) path. Forward ET reaches the LLCT state, which can relax either by back ET (k_{BET} path) from bpy$^{\bullet-}$ to the diimine radical cation or by C-C bond fragmentation of the diimine radical cation (k_{BF} path). From the luminescence and transient absorption studies, it is clear that the forward ET from the MLCT state is very fast; the MLCT emission decays with $k_{FET} = 2 \times 10^9 s^{-1}$, which is nearly 10^3-times faster than the normal MLCT decay rate ($k_d \approx 4.8 \times 10^6 s^{-1}$). The dynamics of triplet→singlet intersystem crossing in the LLCT state may play a role in determining the rate of back ET because it is formed by forward ET from ^{3}MLCT (e.g., ^{3}MLCT→^{3}LLCT). Since the product of back ET has singlet spin multiplicity, intersystem crossing must precede decay of ^{3}LLCT via back ET. It was found that the bond fragmentation competes very effectively with back ET. The rate for bond-fragmentation and back electron transfer are $5 \times 10^5 s^{-1}$ and $8.3 \times 10^7 s^{-1}$, respectively [95].

Another important type of LLCT state arising in diimine rhenium(I) tricarbonyl complexes is found in $IRe^I(CO)_3$(diimine) complexes. When I$^-$ replaces Cl$^-$ or Br$^-$, the lowest excited state changes from being MLCT in nature to that of XLCT (*halide-to-ligand charge transfer*) in character (see Fig. 5) [18, 96]. For the case of $IRe^I(CO)_3$(bpy), a broad but distinct low-energy band appears around 780 nm. In contrast to the above-mentioned LLCT (L to diimine) transitions, which are weak due to the very small electronic coupling between the donor and acceptor, the halide p_y and π^*(diimine) orbitals are now directly coupled by either sharing the
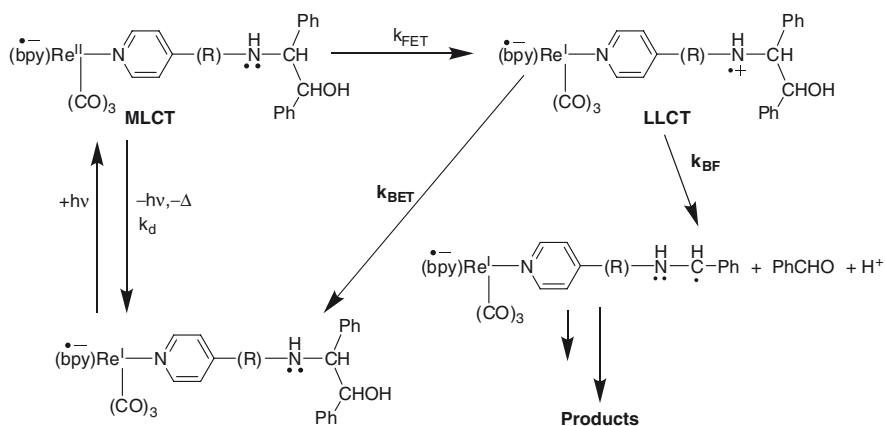

Fig. 4 Excited state dynamics of C–C bond fragmentation (reproduced with permission from [95])
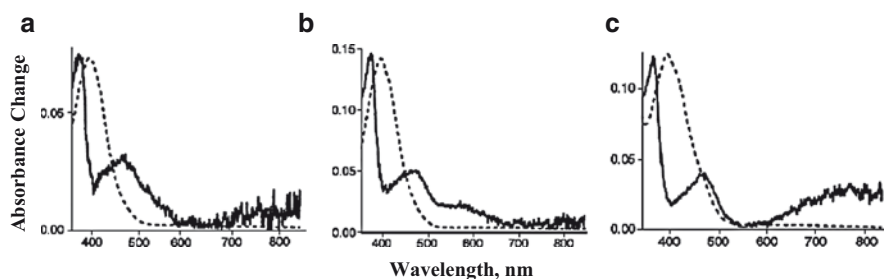
Fig. 5 Ground state (*broken line*) and transient absorption (*solid line*) spectra of Re(X)(CO)$_3$(bpy) in THF measured 10 ns after laser excitation at 460 nm. (**a**) X=Cl, (**b**) X=Br, (**c**) X=I (reproduced with permission from [96])

metal d_{yz} orbital or by through-space p_y–π^* interactions. Thus, XLCT transitions exhibit comparable or slightly weaker intensities compared to MLCT transitions. The XLCT state is a better luminophore because of the higher emission quantum yields and has a longer lifetime compared to the MLCT excited state due to lower nonradiative decay to the ground state. The lifetime of the excited state depends on the diimine ligand which affects both emission and nonradiative decay constant. The MLCT state is more sensitive to the changes of diimine than the XLCT state.

2.3 Complexes with Lowest IL Excited States

Lowest IL states usually occur in complexes containing extended conjugation of the ligands, where the electron is excited predominantly from the ligand-based n- or π-orbitals. Typical characteristics of ^{3}IL emissions are structured profiles and longer emission lifetimes, compared to ^{3}MLCT transitions [97–102]. The emission lifetime is sometimes greatly influenced by temperature or medium effects, though, due to the presence of close-lying ^{3}MLCT states [103]. An early report by Wrighton and coworkers revealed that the complex ClRe(CO)$_3$(3-benzoylpyridine) exhibits typical ^{3}MLCT emission in benzene solution at room temperature [97]. However, in a 77-K EPA glass, the rigidochromic effect shifts the ^{3}MLCT state to higher energy and, thus, multiple emissions from both ^{3}MLCT and ^{3}IL (n–π*) excited states can be observed. Here, the ^{3}MLCT and ^{3}n–π* states are clearly not thermally equilibrated in this glassy environment at low temperature [97]. Many LRe^I(CO)$_3$(X–phen) complexes, where L is a Lewis base and X–phen is phenanthroline or its derivatives, exhibit overlapping emissions from both ^{3}MLCT and ^{3}IL (π →π*) excited states at room temperature. By varying L, X–phen, and temperature, the emitting states can be tuned from ^{3}MLCT to ^{3}π →π* in nature. More structured emissions were observed at 77 K, as well as in complexes with higher ^{3}MLCT excited states [68, 69, 98]. The excited-state decays are also more complicated at low temperature and feature bi- or multiexponential kinetics [99]. Meyer and

coworkers revealed that the observed ^{3}MLCT emission in a system with close-lying ^{3}MLCT and ^{3}IL states does not necessarily prove that the lowest excited state is ^{3}MLCT in character [104]. In the case of *fac*-[ClRe(CO)$_3$(dppz)] (dppz is dipyrido[3,2-a:2′,3′-c]phenazine), the lowest excited state was determined to be the $^3\pi-\pi^*$ excited state by time-resolved resonance Raman spectroscopy, although the emission apparently originates from the ^{3}MLCT excited state. The above chloro complex is a MLCT emitter at room temperature but $\pi\pi^*$ emitter at 77 K. Replacing Cl by PPh$_3$ yields emission originating from the $^3\pi-\pi^*$ state, which is also confirmed by time-resolved resonance Raman spectroscopy [104].

3 Photoinduced Transformations and Chemical Reactions

3.1 Photochemical Ligand Substitution Reactions

Photochemical ligand substitution (PLS) reactions of many transition-metal complexes are known to proceed via a ^{3}LF excited state that is thermally accessible from a ^{3}MLCT state, especially when the photosubstitution involves dissociative mechanisms [105]. The temperature dependence of the emission yield and lifetime of photosubstitution reactions renders an activated process proceeding from ^{3}MLCT to ^{3}LF states, as shown in Fig. 6a. The constants k_{d1} and k_{d2} are nonradiative decay rate constants for the ^{3}MLCT and ^{3}LF states to ground state, respectively. The rate constants k_{th} and k_{-th} are the forward and backward internal conversion rates between the ^{3}MLCT state and the photoexcited state thermally accessible from the ^{3}MLCT state. The thermodynamic analysis of the data unambiguously supports that the photoexcited state is ^{3}LF (see Fig. 6a). There are three possible relaxation pathways
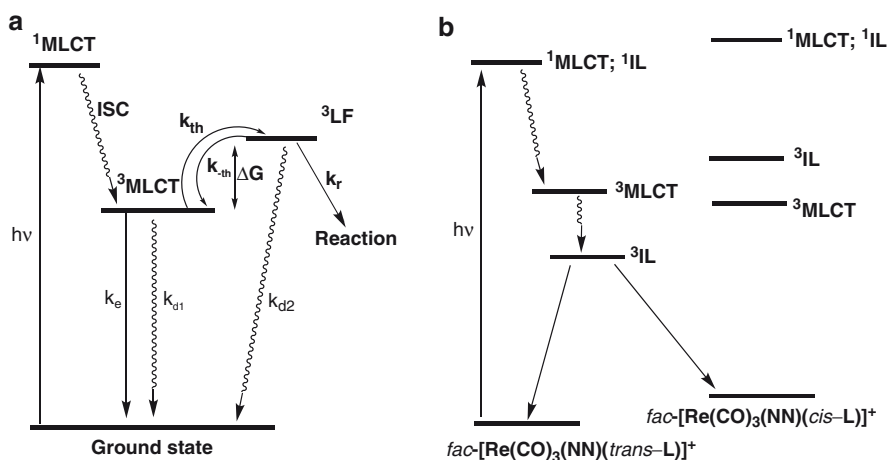

Fig. 6 Simplified energy diagram describing the mechanism of the (**a**) PLS reaction of *fac*-[Re^I(bpy)(CO)$_3$(PR$_3$)]$^+$ and (**b**) *trans-cis* isomerization of *fac*-[Re^I(NN)(CO)$_3$(L)]$^+$

through the ^{3}LF state: (1) photodissociation that gives reaction products, (2) photo-dissociation and successive recombination, and (3) direct nonradiative decay to the ground state. Both the nonradiative decay and reaction pathways from the ^{3}LF state are extremely fast with rate constants $> 10^{14}$ s^{-1}, and this suggests that the ^{3}LF excited states of the complexes have repulsive potential curves and that the temperature-dependent nonradiative decay processes proceed via CO ligand dissociation and successive recombination of the produced species in rhenium(I) diimine complexes of the type [Re(X$_2$bpy)(CO)$_2$(PR$_3$)]$^+$ [106].

Many complexes of the type Re(bpy)(CO)$_3$L, where L is a weak field ligand like pyridine or halide, are photostable to irradiation into the MLCT manifold. Efficient photochemical ligand substitution is found for *fac*–[Re(X$_2$bpy)(CO)$_3$(PR$_3$)]$^+$ to yield substitution *trans* to the axial PR$_3$ group by CO loss (X$_2$bpy is 4,4′-X$_2$ −2,2′-bpy, where X is H, CF$_3$, OEt or Ph, and PR$_3$ is a tertiary phosphine or phosphite) and the biscarbonylrhenium(I) diimine complexes, *cis-trans*-[Re(X$_2$bpy)(CO)$_2$(PR$_3$)L]$^{n+}$, were formed with chloride, py or CH$_3$CN as the entering group [107]. The activation energies for photosubstitution were found to be between 3,200 and 4,800 cm^{-1}, and photosubstitution yields were generally in the range of 0.1–0.55. Labeling (^{13}CO) studies demonstrated that the axial CO, which is *trans* to the phosphorus ligand, was indeed labilized, consistent with a dissociative mechanism and an associated excited-state kinetic *trans*-effect [106].

The photostability of *fac*–[Re(bpy)(CO)$_3$py]$^+$, *fac*–[Re(bpy)(CO)$_3$Cl], or related bipyridyl-substituted complexes is proposed to be due to the weaker *trans*-labilizing ability of the py or chloride ligand compared to a phosphorus donor, and not because of a larger activation energy being required to reach the ^{3}LF state. For the *fac*–[Re(bpy)(CO)$_3$(PEt$_3$)]$^+$ complex, both possible *trans*-axial labilization products are observed in CH$_3$CN solution, i.e., *trans* to axial-phosphine as well as *trans* to axial-CO labilized substitutions, and Re(bpy)(CO)$_2$(PEt$_3$)(CH$_3$CN)$^+$ and Re(bpy)(CO)$_3$(CH$_3$CN)$^+$ are found in a 2:1 ratio. This may indicate that the kinetic *trans*-effect of the triethylphosphine group and CO is comparable [108].

Ishitani et al. reported that the PLS reactions of *fac*–[Re(4,4′-X$_2$-bpy)(CO)$_3$Cl] (X = H, MeO, NH$_2$, CF$_3$) are induced by high-energy (UV light) photoexcitation and yielded solvato complexes, *fac*–[Re(4,4′-X$_2$-bpy)(CO)$_2$(solvent)Cl] [109]. The fact that the PLS reaction rate was not affected by the presence of O$_2$, but the emission was efficiently quenched with a rate constant of 3.6×10^9 M^{-1} s^{-1} by O$_2$, reveals that the PLS reaction does not occur from the emissive state. Mechanistic studies, including TRIR measurements, clearly reveal that the PLS reaction does not proceed via the lowest ^{3}MLCT state, but instead it occurs via higher vibrational levels of the ^{1}MLCT and/or higher electronic states, such as $^1\pi\rightarrow\pi^*$, and higher-lying Re→bpy and Re→CO ^{1}MLCT states. The TRIR measurements have indicated that the CO ligand dissociates with subpicosecond rates after excitation, leading to vibrationally hot CO-loss photoproducts (with a very broad TRIR band) after 1 ps of excitation and the relaxed photoproduct (with a distinct TRIR band) forms during 50–100 ps after excitation [109].

Photosubstitution of diphosphine-bridged bimetallic complexes utilizes 1,2-*trans*-bis-diphenylphosphinoethylene as the bridging ligand and yields only *trans*-substituted

products with quantum yields as high as 0.35 [110]. This is proposed to be due to self-quenching, i.e., intramolecular energy transfer from the high-energy chromophore that proceeds efficiently to the low-energy photostable ligand-substituted chromophore. In fact, TRIR studies have demonstrated this rapid energy transfer by monitoring the change in the ground and excited-state Re-CO modes.

The homolysis of the metal–alkyl bond for $[Re(R)(CO)_3(diimine)]$ ($R = CH_3$ and C_2H_5) is also reported [111, 112]. The optical excitation of an CH_3CN solution of $[Re(Et)(CO)_3(dmb)]$, where dmb is 4,4′-dimethyl-2,2′-bipyridine, produces within 2 ps the radicals $Et^·$ and $[Re(MeCN)(CO)_3(dmb)]^·$ together with an excited state, which undergoes a slower (~90 ps) conversion to the same radicals. The photoactive excited state was identified as ^{3}MLCT with an admixture of ^{3}SBLCT (*sigma bond-to-ligand charge transfer*) character [112]. For the ethyl complex, ^{3}SBLCT is the lowest state, while in the methyl complex, this lies above both the singlet and triplet MLCT states. The excited state decay of $[Re(C_2H_5)(CO)_3(dmb)]$ led only to homolytic cleavage of the $Re–C_2H_5$ bond, whereas for $[Re(CH_3)(CO)_3(dmb)]$, both homolytic cleavage of the $Re–CH_3$ bond and decay from the excited state to the ground state occurred in a 1:1 ratio.

3.2 Photoinduced cis-trans Isomerization Reactions

Complexes incorporating a ligand with a lowest nonemissive ^{3}IL excited state that is energetically tunable by a light-induced structural change (such as in stilbene or azobenzene derivatives) have potential applications as light-switching materials. When the olefin or azo groups are in *trans*-conformations, the complexes are weakly or nonemissive due to the presence of lowest nonemissive $^3\pi–\pi^*$ or ^{3}n–π^* excited states. Excitation into their ^{3}MLCT excited state sensitizes the $^3\pi–\pi^*$ or ^{3}n–π^* excited states and results in *trans-cis* isomerization of the ligand. The $^3\pi–\pi^*$ or ^{3}n–π^* excited states in the *cis*-conformer are shifted to a higher energy position compared to the emissive ^{3}MLCT state and, consequently, strong emission is observed [36–38]. Figure 6b depicts the simplified energy diagram of *trans-cis* isomerization. Figure 7 represents the processes involved in the *trans*-to-*cis* isomerization of azo and ethylene linkages associated with complexes of the type
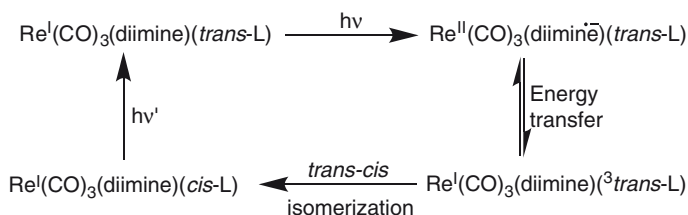

Fig. 7 Photoinduced *cis-trans* isomerization of complexes with olefin or azo linkages

[Re(diimine)(CO)$_3$L]$^+$, where L is the ligands shown in Fig. 8a. To achieve the reverse process of *cis* to *trans* isomerization, requires exciting the complexes at higher energy than the energy needed to cause *trans*-to-*cis* isomerization [113, 114]. The reversible *trans*-to-*cis* and *cis*-to-*trans* behavior resulting from excitations at differing frequencies was equated to a "*light-controlled photoswitch.*" Several reports have taken advantage of this unique property to design a variety of photoswitching systems in recent years [36–43].

Gray et al. reported the *cis-trans* photoisomerization of [Re(phen)(CO)$_3$L$_1$](PF$_6$) [113]. The [Re(phen)(CO)$_3$(*cis*-L$_1$)](PF$_6$) complex exhibits yellow luminescence after UV excitation, whereas the *trans*-counterpart, [Re(phen)(CO)$_3$(*trans*-L$_1$)] (PF$_6$), is nonluminescent. Irradiation at 350 nm causes *trans*-to-*cis* isomerization while the reverse *cis*-to-*trans* isomerization was achieved by irradiating at 250 nm. [Re(diimine)(L$_3$)(CO)$_3$]Cl complexes undergo reversible isomerization upon alternate irradiation at 365 nm and 254 nm [114]. The intense absorption band centered ca. 350–380 nm decreases in intensity upon irradiation at ca. 365 nm and recovers upon irradiation at ca. 254 nm. These changes are attributed to the *trans*-to-*cis* isomerization of the –CH=CH– moiety. For the azo-group containing complexes [Re(diimine)(azo-L$_3$)(CO)$_3$]Cl, reversible electronic absorption spectral changes were observed in degassed dichloromethane solution upon alternate irradiation at 365 and 450 nm. The spectral changes are suggested to be associated with the *trans-cis* isomerization of the –N=N– moiety.

Coordination of an azobenzene-like ligand to the Re^I center accelerates the singlet→triplet state intersystem crossing from optically prepared Franck-Condon states (for example, $^1\pi\pi^*$, ^{1}MLCT, and $^1n\pi^*$) in femtosecond time domain, thereby switching the *trans-cis* isomerization mechanism to the $^3n\pi^*$ potential energy surface. The Re^I moiety acts as an intramolecular triplet sensitizer. The ^{3}MLCT(bpy) state of *fac*–[Re(bpy)(CO)$_3$L$_2$]$^+$ undergoes a 3 ps conversion to the reactive intraligand $^3n\pi^*$ excited state. The isomerization of –N=N– is about 200-times faster than the isomerization of the –C=C– bond from the $^3\pi\pi^*$ state of the analogous Re(I) styrylpyridine complexes [115].

Moore and coworkers reported one particularly interesting proton-induced photoisomerization of the *fac*–[Re^I(bpy)(L$_4$)(CO)$_3$]$^+$ chromophore at the stilbene-like bridging ligand, because the intramolecular energy-transfer is feasible after protonation of the azacrown ether [39]. The absorption spectra of the *trans*-conformer *fac*–[Re^I(bpy)(*trans*-L$_4$)(CO)$_3$]$^+$ feature the dπ(Re)→π^*(bpy) MLCT band at ca. 380 nm and an intense ILCT band at ca. 435 nm, localized on the azacrown ligand L$_4$, in which charge is transferred from azacrown ether nitrogen to the pyridyl N-atom acceptor. The ILCT band is blue shifted to ca. 320 nm in the protonated complex, owing to the protonated azacrown ether at the N-atom inhibiting the charge transfer and raising the energy level of the ILCT excited state. The complex is only weakly emissive at room temperature in both the protonated and nonprotonated forms. Prolonged irradiation of the complex shows no spectral changes, while the protonated complex shows pronounced spectral changes in absorption and enhanced emission intensity (see Fig. 8b). This is consistent with efficient *trans*-to-*cis* photoisomerization at the olefin bond in the protonated form of the complex.
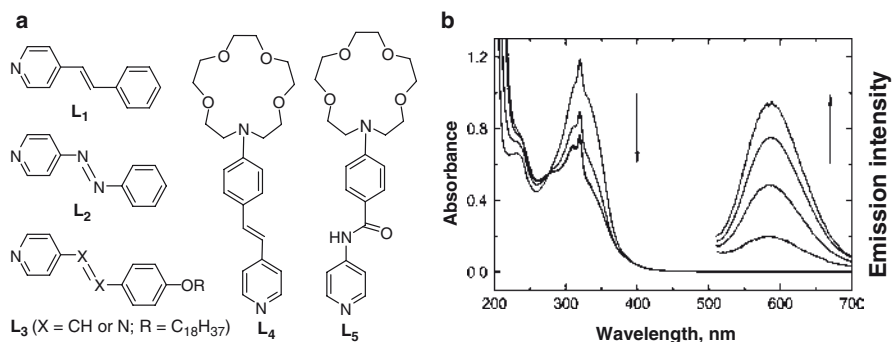
Fig. 8 (**a**) Azo, ethylenic, and crown ligands studied for photoswitch and isomerization and (**b**) absorption spectra of *fac*-[Re^I(CO)$_3$(bpy)(*trans*-L$_4$)]$^+$ in CH$_3$CN with excess HCl added after irradiation at 406.7 nm for 0, 30, 120, and 180 min, along with corresponding emission obtained on excitation at 380 nm (no distinct emission features were observed at wavelengths lower than 500 nm) (reproduced with permission from [39])

The increase in emission intensity of the protonated species can be attributed to a reduction in the intramolecular energy-transfer decay after isomerization to the *cis*-complex, reflecting the higher energy position of the $^3\pi - \pi^*$ states compared to the ^{3}MLCT states in the *cis*-styryl pyridine complex [39].

An interesting light-controlled alkali and alkaline earth metal ion switching was observed for the complex [Re^I(CO)$_3$(bpy)L$_5$]$^+$, where L$_5$ contains an azacrown ether [116]. It can release the ion in nanoseconds and recapture it in microseconds. The emission from the complex [Re^I(CO)$_3$(bpy)L$_5$]$^+$ is very weak and has a very short life of $\tau_{em} < 1$ ns, due to rapid quenching of the MLCT state by electron transfer from the LLCT state, with $\tau_{FET} = 500$ ps (see Fig. 9). The complex shows an intense band at 344 nm, which has been assigned to an ILCT transition, in which charge is transferred from the azacrown electron donor to the amidopyridyl electron acceptor. A weak MLCT band at 350 nm appears as a shoulder to this ILCT band. The addition of acid or metal salts results in a blue-shift of the ILCT band, with a large shift occurring on protonation. This is attributed to the interaction of the cation with the azacrown nitrogen atom, increasing its oxidation potential by raising the energy of the ILCT transition. The emission quantum yield and lifetime are increased on forming the [Re(CO)$_3$(bpy)L$_5$]$^+$–H$^+$ and –M^{n+} complexes. Protonation substantially increases the MLCT emission yield and lifetime by raising the energy of the LLCT state so effectively that all of the photophysics occurs via the MLCT state. Photoexcitation to the MLCT state of the metal ion-complexed form, [Re(CO)$_3$(bpy)L$_5$]$^+$–M^{n+} (M^{n+} = Li$^+$, Na$^+$, Ca^{2+}, or Ba^{2+}), results in cation release and, after decay to ground state, [Re(CO)$_3$(bpy)L$_5$]$^+$ recaptures the metal cation to restore the starting thermal equilibrium (see Fig. 9).
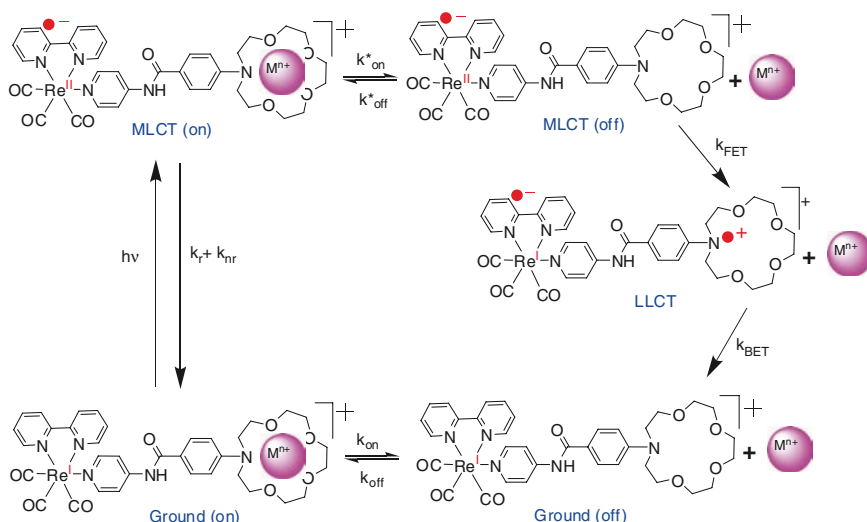
Fig. 9 General mechanism for light-controlled ion switching in the *fac*-[Re^I(CO)$_3$(bpy)L$_5$] complex

Yam's group have studied the photosensitized intramolecular ring-opening [117, 118] and ring closing [119–121] of rhenium complexes containing spirooxazine and diarylethene moieties attached to either pyridine or diimine ligands (see Fig. 10). The ring-closing process of the complexes proceeds initially with formation of the ^{1}MLCT state, which undergoes intersystem crossing to the ^{3}MLCT excited state ($\tau \leq 0.8$ ps). The ^{3}MLCT excited state then undergoes internal conversion or intramolecular energy transfer to produce the ^{3}IL excited state ($\tau \approx 1.8$ ns), which subsequently initiates the formation of the closed form of the complexes ($\tau \approx 7$ ns). In the case of complex **5** (see Fig. 10), excitation into either the IL or MLCT band of the open form in chloroform resulted in light emission with a maximum at 570 nm, which can be assigned as ^{3}MLCT phosphorescence [119]. Upon prolonged excitation at the isosbestic point ($\lambda = 352$ nm) of the complex **5**, photocyclization took place and the emission intensity at ca. 570 nm was found to decrease, indicating photoisomerization. Complex **5** shows an intense IL absorption band at ca. 352 nm and a shoulder at ca. 425 nm, which was ascribed to a MLCT [dπ(Re)→π*(ligand)] transition, with some mixing of a metal-perturbed IL (π→π*) transition. Interestingly, upon UV excitation at $\lambda \leq 450$ nm into either the IL or MLCT bands, three absorption bands were generated at ca. 290, 480, and 713 nm (see Fig. 10c). This new set of absorption bands were assigned as metal-perturbed ^{1}IL transitions with mixing of ^{1}MLCT transitions in the longest wavelength absorption band originating from the ring-closed form of the complex **6**. Such a large shift of the absorption band of the cyclized form of complex **6** to the NIR region could be attributed to the planarization of the four heterocyclic rings relative to the open forms.

Thus, contrary to the twisted conformation of the ligand, the coordination of the rhenium(I) metal center forces the 2,2′-linked pyridyl and imidazoyl rings into coplanarity from their twisted conformation, causing an increase in the extent of
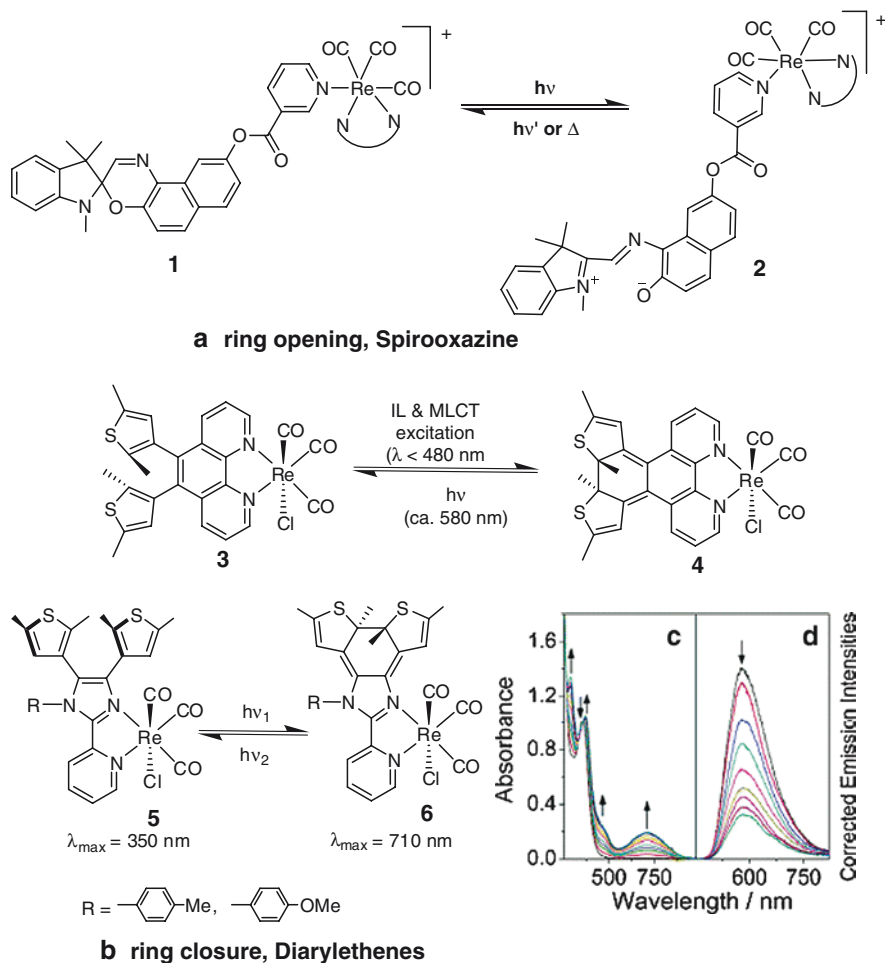
a ring opening, Spirooxazine

b ring closure, Diarylethenes

Fig. 10 Photoinduced ring opening (**a**) and ring closing (**b**) mechanisms. *Inset* shows UV–Vis absorption (**c**) and corrected emission spectral changes (**d**) of **5** in chloroform upon MLCT excitation at 410 nm at 298 K (reproduced with permission from [119])

π-conjugation. Upon photocyclization, the extent of π-conjugation in closed forms is further enhanced leading to absorption in the NIR region. In addition, excitation into the MLCT absorption band also triggered photocyclization of the open forms, implying that the photocyclization can occur via MLCT excited-state photosensitization. Upon excitation into the bands of the closed forms of complex **5**, the photochromic backward reaction took place. The quantum yield for photocyclization (ca. $\Phi_{350} = 0.4$) is much higher than the photocycloreversion reaction (ca. $\Phi_{510} = 0.004$) [119].

Unlike most metal complexes containing the *fac*–(diimine)Re^I(CO)$_3$ unit, which are typically highly luminescent in solution, trinuclear rhenium carbonyl compounds **7** and **8** (see Fig. 11a) show only weak luminescence ($\Phi_{em} = 0.0015$) in CH$_3$CN at room temperature [36]. The quenching appears to occur via intramolecular
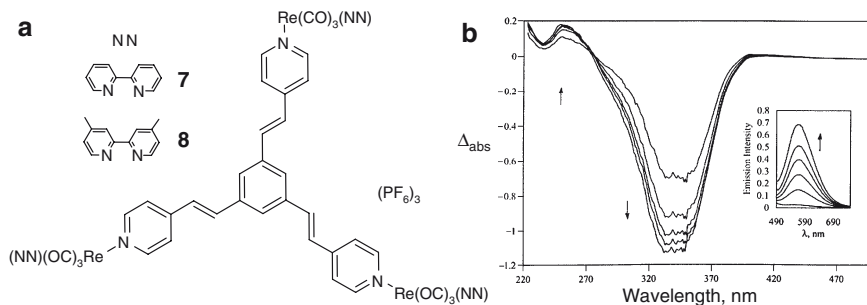
Fig. 11 (**a**) Trinuclear rhenium carbonyl complexes **7** and **8** and (**b**) UV–Vis difference spectra ($\Delta_{abs} = A_t - A_{t=0}$) of compound **7** in CH_3CN at 293 K after irradiation at 366 nm for 0, 1, 2, 3, 4, 6 h, and *inset* shows the emission spectral changes before and after photolysis (reproduced with permission from [39])

sensitization of the $\pi \to \pi^*$ transitions localized on the olefin link of the bridging ligand. Prolonged photolysis into the MLCT band at 366 nm, bleaches the $\pi \to \pi^*$ absorption of the bridging ligand at ca. 280–370 nm with concomitant appearance of new bands at ca. 200–270 nm and an enhancement in the emission intensity (see Fig. 11b). The determined emission quantum yields for complexes **7** and **8** are 18 and 21 times increased after 7 h photolysis at 366 nm, respectively. The UV-Vis spectral changes and large increase in the luminescence intensities for **7** and **8** are consistent with the *trans-to-cis* isomerization of the olefinic bond. Therefore, the nonradiative decay of energy is inhibited and highly efficient energy transfer from the [3]MLCT to [3]LF state occurs, which triggers the *trans*-to-*cis* isomerization at olefinic bonds in the complex.

4 Metal-Directed Macrocyclic Complexes Incorporating Diimine Rhenium Tricarbonyl Moieties

4.1 Photophysical Properties

In general, Re(I) complexes form corners of triangles, squares, and rectangles [27, 122–140], and the squares **14** and **15** contain two Re and two Pd/Pt complexes in opposite corners [132, 133]. Though, the spacers holding the metal centers in place are mostly based on ligands containing pyridine functionalities on opposite ends of an organic linker, diimine bridges [130, 131], alkoxides [122, 123], and hydroxyquinones [125] have also been reported. Bridging ligands containing a metal complex resulting in additional metal centers to the squares **13m**, **14m**, and **19** were also studied [129–131, 135–137]. A cage-like hexanuclear rhenium molecular prism **21** has also been reported [141–143]. Figure 12 lists metal-directed molecular
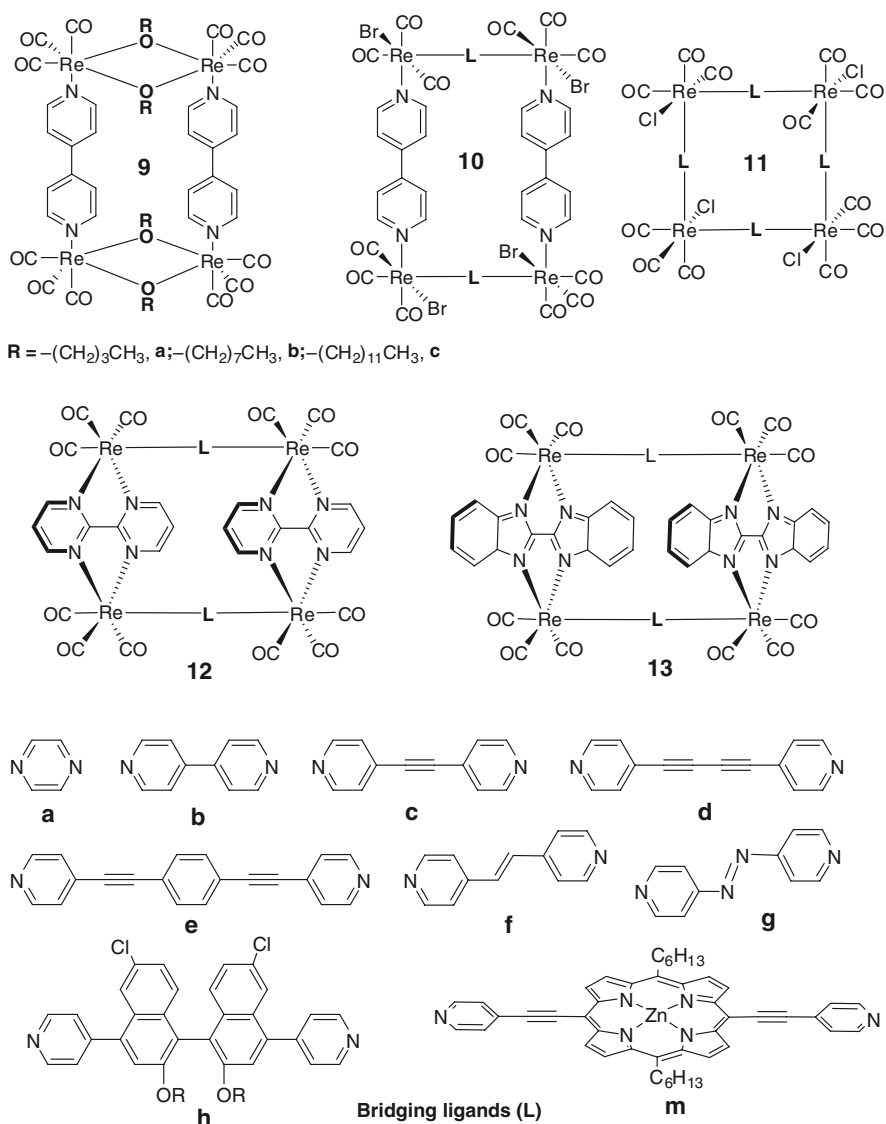
R = −(CH₂)₃CH₃, **a**; −(CH₂)₇CH₃, **b**; −(CH₂)₁₁CH₃, **c**

R = $-(CH_2)_3CH_3$, **a**; $-(CH_2)_7CH_3$, **b**; $-(CH_2)_{11}CH_3$, **c**

Fig. 12 Supramolecular metallacyclic rhenium(I) tricarbonyl diimine complexes

assemblies of Re(I) diimine complexes in various geometries, such as triangles, squares, rectangles, etc. In general, the absorption spectra of rhenium carbonyl-based metallacycles exhibit two main features that are assigned as bridging-ligand localized $\pi \rightarrow \pi^*$ and MLCT transitions and the emission intensity is significantly diminished to that of the mononuclear rhenium complexes. The diminished luminescence can be attributed to a decrease in the emission lifetime, thought to be quenched by the additional vibronic components.
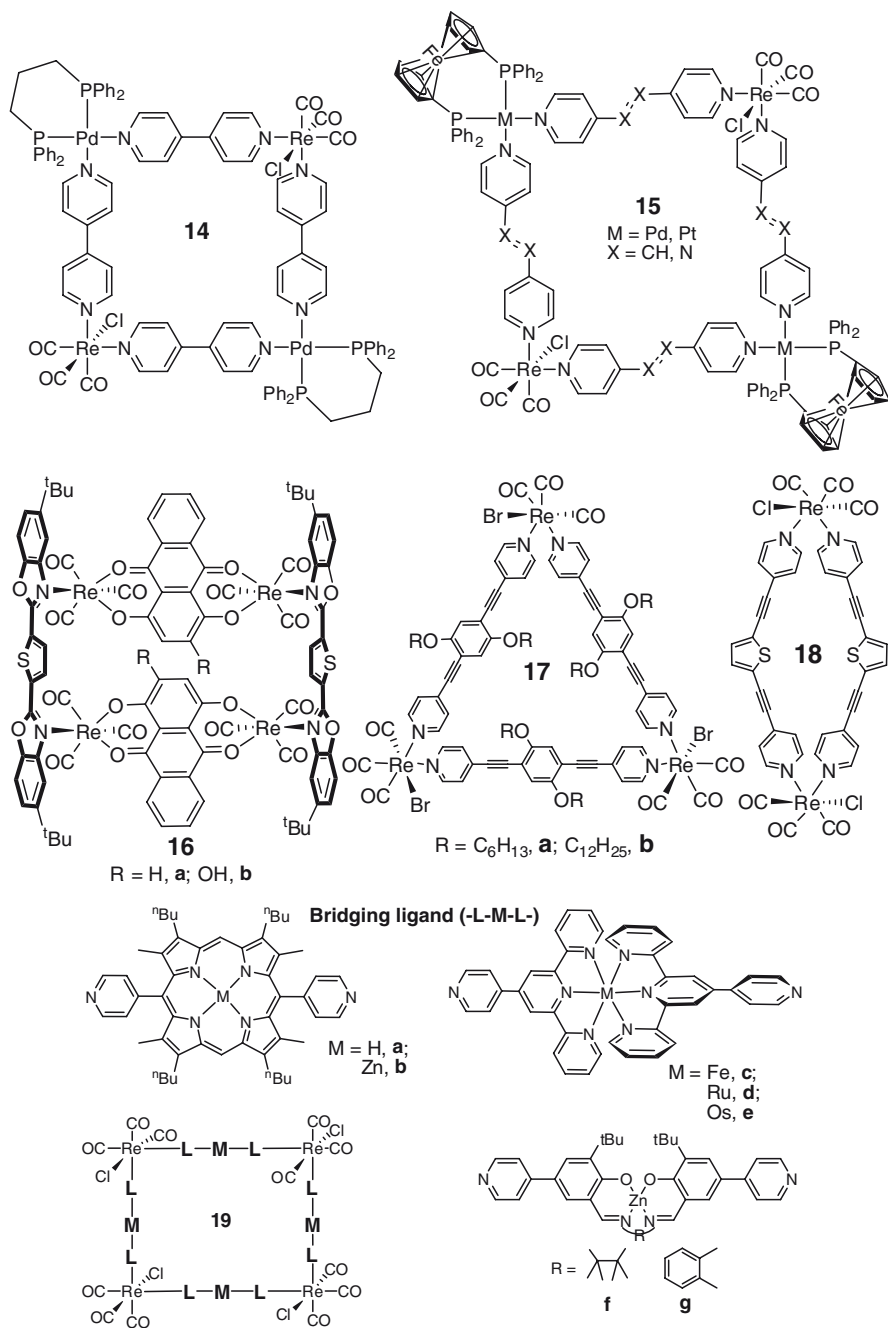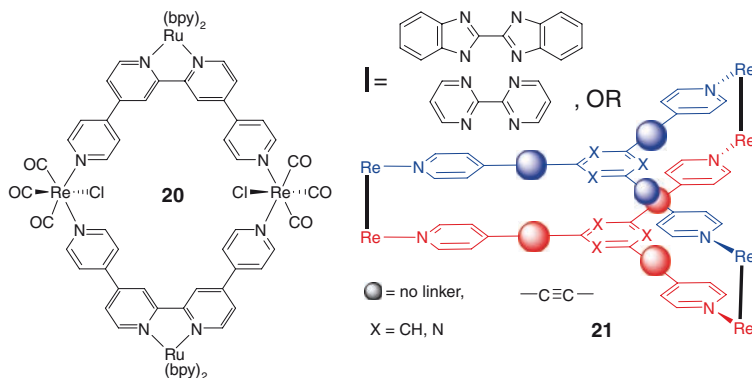
Fig. 12 (continued)

Fig. 12 (continued)

The MLCT band and emission maximum of rectangle **9c** were located near 385 nm and 600 nm, respectively [122]. The emission intensity was dependent on the solvent. The quantum efficiency and lifetime increased from 0.39×10^{-3} and 0.39 ns in CH_3CN to 6.54×10^{-3} and 212 ns in a 1:9 $CH_3CN:H_2O$ mixture, owing to aggregation in the presence of water. Other rectangles **9** having linkers (R = H, CH_3, CH_2CH_2OH) were not emissive in solution at room temperature [122, 123]. The intense absorption maxima at ~350 nm was observed for rectangle **10**, which is ascribed to spin-allowed MLCT from the Re_d orbital to the π^* orbital of the ligand, and the high-energy band ca. 260 nm is assigned to the ligand-centered transitions. Emission maxima for rectangle **10** in CH_2Cl_2 were located near 600 nm and the emission lifetimes varied from 86 to 495 ns for **10c**, **10d**, and **10e** [124]. The exceptionally longer lifetime for **10e** is probably due to the involvement of the extended π-system of the bridging ligand.

The electronic absorption of square **11** is contained with two main features of bridging-ligand localized $\pi \rightarrow \pi^*$ and MLCT transitions [125–128]. In square **11a**, **11b** the lowest-energy band is solely of MLCT character, while in the other squares **11c-f**, the $\pi \rightarrow \pi^*$ and MLCT bands are substantially overlapping. Square **11d** gave the characteristic ^{3}MLCT emission of Re(diimine)(CO)$_3$Cl complexes located at 635 nm with a short emission lifetime of 39 ns and a low emission quantum yield of 8.5×10^{-4} [127, 128]. The MLCT band in square **11d** is bathochromically shifted by 1,385 cm^{-1} to that of its corner complex because of additional conjugation. The shorter lifetime of the square to its corner is attributed to an enhanced nonradiative decay rate of the square, due to the lower energy of the excited state and more effective vibronic coupling [20]. The square **11g** shows an additional low-energy $n \rightarrow \pi^*$ transition that originates from the *trans*-azp ligand (azp = 4,4′-azobipyridine), which is overlapped by a MLCT transition. Square **11d** exhibits ^{3}MLCT emission at ca. 635 nm, which is independent of excitation wavelength, with an emission lifetime of 39 ns in THF at ambient temperature. In contrast, the square **11g** is nonluminescent owing to effective intramolecular energy transfer from the initially

formed ^{1,3}MLCT excited states to the lowest nonemitting n→π* state [41]. The luminescent metallacycles **11h** exhibit electronic absorption bands at ca. 245, 305, and 360 nm in the UV region originating from the ligand π→π* transitions and additional bands at ca. 325 nm, which are probably due to the MLCT transitions [129]. The square **11h** shows two luminescence peaks ca. 412 and 536 nm in THF when excited at 360 nm. The emission peak at 412 nm can be assigned to a ligand-localized π→π* excited state, while the weaker emission at 536 nm is due to a ^{3}MLCT excited state.

Molecular rectangle **12a** shows a solvatochromic absorption MLCT band at 490, 484, and 450 nm in H_2O, DMSO, and CH_3CN, respectively, due to dπ(Re)→π*(bpm) charge-transfer transitions [130]. These rectangles are not emissive at room temperature, in agreement with results reported for the monomer, [Re(bpm)(CO)$_3$Cl] (bpm = 2,2′-bipyrimidine), which is also nonluminescent [131]. The UV–Vis spectrum of rectangle **13b** shows a band in the high-energy region, which is absent in the dinuclear benzimidazole (biz), $Re_2(CO)_6(biz)_2$ complex. This band is ascribed to the allowed dπ(Re)→π*(bpy) singlet charge transfer [132]. Unlike **12b** or other pyrimidine-edged rectangles, **13b** luminesces in solution at ca. 617 nm in tetrahydrofuran and in the solid state at ca. 572 nm. The emission lifetime varies in the range 26 ns (CHCl$_3$) to 238 ns (THF/MeOH) depending on the solvent. Owing to its long lifetime and large Stokes shift, the emission was attributed to predominantly originating from triplet charge-transfer state(s). The visible region spectra of molecular rectangles **12m** and **13m** are dominated by porphyrin-based B- and Q-bands. In particular the Q-bands for both molecular assemblies are bathochromically shifted ca. 20 and 10 nm to that of porphyrin bridge, respectively [133]. This red shifting is consistent with electron-withdrawing effects due to metal-cation coordination. Both rectangular metallacycles **12m** and **13m** show red-shifted singlet emission maxima compared to the porphyrin bridging complex at ca. 694 and 714 nm, respectively. Interestingly, the emission from the rectangle **13m** occurs from a singlet state, which is ca. 3,000 cm^{-1} higher in energy than the usual MLCT emission of Re^I(diimine)(CO)$_3$ complexes.

The luminescent heterometallasquare (Re/Pd) **14** showed emission from the ^{3}MLCT state with a maximum at ∼625 nm and an emission lifetime of 17 ns in deoxygenated acetone [134]. The luminescence intensity was decreased by ca. 25-fold after the square formation. This quenching of luminescence was attributed to the Pd(II) fragment. The square **15**, containing azp as the bridging ligand, shows high-energy bands below 300 nm, which are assigned to azp-localized π→π* transitions and a broad shoulder at ca. 380 nm, which is assigned to dπ(Re)→π*(azp) MLCT [135]. The very weak absorption band that tails into the visible region comprises azp-localized n→π*, Pd-centered LF, and Fe-centered LF absorptions. The 4,4′-ethenylbipyridine (bpe) linked square **15** show bands that are characteristic of both *cis-* and *trans*-bpe. The *trans*-bpe-**15** square exhibits a band at ca. 300 nm that extends into the visible region, while the *cis*-bpe-**15** complex displays a blue-shifted band at ca. 290 nm [135]. No luminescence was observed for square **15** because of the proximity of close-lying Pd- and Fe-localized LF bands to the lowest excited state(s) that provide rapid nonradiative decay to the ground state.

The gondola-shaped molecular rectangle **16** displayed an intense absorption band in the region 230–395 nm and a weak shoulder at ca. 420 nm, which are ascribed to $\pi\to\pi^*$ and MLCT transitions, respectively [136]. It also shows weak intraligand absorptions at ca. 585 and 632 nm, originating from anthraquinone bridging ligands. A set of structured emissions appeared at ca. 438 nm with high quantum yields of 0.719 for **16a** and 0.379 for **16b**. The small Stokes shift and short lifetime of **16a** indicate that the emission originates from a singlet $\pi\to\pi^*$ state. Solid-state emission centered at ca. 448 and 518 nm for **16a** is attributed to the decay of the $\pi\to\pi^*$ excited state of the bridging benzooxazolylthiophene (bzt) ligand and $d\pi(Re)\to\pi^*(bzt)$ excited state, respectively [136].

The absorption spectrum of triangle **17a** exhibits two broad bands at 329 and 422 nm [127]. The lowest-energy band is assigned to a mixture of MLCT and $\pi\to\pi^*$ excited states. The room-temperature emission spectrum of triangle **17** in $ClCH_2CH_2Cl$ exhibits structured features with maxima at 499 and 476 nm (for **17a**) and 512 and 470 nm (for **17b**). The low-temperature emission spectrum of **17a** displays more distinct structure with bands at 463, 488, 520, and 549 nm (an average spacing of 1,188 cm^{-1}) in 2-methyltetrahydrofuran. These observations illustrate that the dual emission bands are actually a vibronic structure form of the $\pi\to\pi^*$ excited state. A very small blue shift on going from the solution to a rigid glass also supports the assignment that the emission occurs from a ligand-based $\pi\to\pi^*$ excited state [7, 8]. The extremely short lifetime (ca. 360 ps) and relatively high-energy emission from **17a** ($\Phi_{em} = 0.032$) indicate that the emission is apparently ligand-localized $^1\pi\to\pi^*$. However, the fast radiative decay rate ($k_r \sim 10^8$ s^{-1}) from the $^1\pi\to\pi^*$ excited state localized on the corresponding bridging ligand implies that the fluorescence is still able to compete with the other nonradiative decay processes. The folding motions of the hexyloxy chains in **17a** are believed to be responsible for the rapid vibrational relaxation from the ^{3}MLCT excited state. In fact, except for the vibronic structures observed at high-energy positions, a very weak emission centered at 602 nm with lifetime 163 μs was also observed at 77 K glass. This band is assigned as a ^{3}MLCT transition on the basis of the absence of vibrational structure, although some involvement of $^3\pi\to\pi^*$ character cannot be completely ruled out.

The absorption spectrum of the dinuclear complex **18** features a broad band centered at 383 nm and a shoulder at 422 nm [126]. The low-energy shoulder is assigned to be MLCT in character and the band at 383 nm is assigned to the ligand localized $\pi\to\pi^*$ transitions and no luminescence was observed from **18** in CH_2Cl_2 solution. The square assembly of porphyrins **19a, b** is highly soluble in CH_2Cl_2 but insoluble in water and highly chromophoric in the porphyrin Soret region, ca. 400–420 nm [137]. The square formation induces a bathochromic shift of ca. 6 nm in the Soret region because of rhenium-pyridine coordination. Near-UV fluorescence excitation studies suggest that rhenium corners serve only a structural rather than a direct photophysical role within the square framework. Single photon counting experiments yielded excited-state lifetimes of 3.0 ns for **19a** and 2.4 ns for **19b**. The squares **19c, d, e** display broad and intense visible absorptions in the region 400–600 nm, which are assigned to metal (Fe, Ru, or Os)-to-ligand (pytpy) MLCT

transitions [138]. Square **19e** exhibits an additional weak band at ca. 676 nm which is assigned to an Os^{-3}MLCT band. The bands centered between 279 and 377 nm are assigned to ligand π–π* bands and the Re-based MLCT band. Though, the corresponding corner Re(CO)$_3$(pytpy) (pytpy = 4′-pyridyl-2,2′;6′,2″-terpyridine) exhibits ^{3}MLCT luminescence at ca. 530 nm in CH$_3$CN with a lifetime of 646 ns, the squares **19c** and **19d** do not have any detectable luminescence at room temperature.

The lack of luminescence from squares **19c** and **19d** is attributed to the existence of metal-centered (MC) states lying in close proximity to the MLCT states [14]. The square **19e** exhibits room-temperature luminescence in deoxygenated CH$_3$CN solution at ca. 748 nm with a shorter lifetime ca. 42 ns and lower quantum yield 4.2 × 10^{-4} compared with its bridging unit Os(pytpy)$_2$. The origin of the emission is assigned to Os(II)-based ^{3}MLCT transitions. The stronger ligand field and lower oxidation potential of Os(II), compared with Ru(II) and Fe(II), results in an increased energy gap between the ^{3}MLCT and ^{3}MC states [14]. Further, the excitation of square **19e** at 380 nm, where the Re(I) moiety is the sole chromophore, and the excitation at 490 nm resulted in the same emission maxima. This lack of excitation wavelength dependence implies that the energy transfer from higher-energy state(s) (Re-MLCT or π–π*)-to-lowest Os-^{3}MLCT state(s) is very efficient. The spectral overlap between the absorption band of square **19e** and the emission from its corresponding corner Re(CO)$_3$(pytpy)$_2$Br occurs from the red edge of the singlet absorption band to the triplet absorption band. This kind of overlap of absorption bands implies that the intramolecular energy transfer is most likely to be a triplet to triplet process. The incorporation of the Zn-salen complex into molecular squares **19f** and **19g** results in only subtle changes in visible-region characteristics, indicating little contribution from the Re^I charge transfer [139]. The slight blue shift of emission maxima and modest decrease of lifetime for both squares **19f** (λ_{em} = 460 nm, Φ_{em} = 0.039, τ_{em} = 0.50 ns) and **19g** (λ_{em} = 526 nm, Φ_{em} = 0.073, τ_{em} = 0.62 ns) compared to their Zn-salen bridging unit implies that there is enhanced intersystem crossing to nonemissive triplet state(s).

The heterometallacyclic assembly **20** shows high intensity-high energy bands which are consistent with intraligand π→π* transitions. The band at ca. 470 nm is assigned to Ru(dπ)→L(π*) MLCT transitions, while the band centered at ca. 363 nm is attributed to Re(dπ)→L(π*) MLCT transitions [140]. The complex exhibits intense emission centered at ca. 665 nm in aqueous and organic solvents, which is assigned as emission from Ru-MLCT. Interestingly, the emission is independent of the excitation wavelength, implying that the energy transfer within the macrocycle is efficient and that the excitation into any MLCT or π–π* excited state results in relaxation to the lowest lying Ru-MLCT state.

The molecular prism **21**, held with 2,2′-bipyrimidine, features intense bands in the near-UV region and a low-energy band at ca. 470 nm, tailing past 600 nm in CH$_3$CN. This low-energy band is assigned to the dπ(Re)→π*(bpm) MLCT [140]. It shows no detectable emission in CH$_3$CN solution at room temperature. The alkoxide-bridged neutral prism **21** shows an extended solvochromic MLCT band at ca. 549 nm in CCl$_4$, 488 nm in CH$_3$CN, and 424 nm in DMSO [141]. Hupp et al. studied the redox behavior of the prism **21** bridged with 2,2′-bisbenzimidazole

(biz) [142]. The reduction of **biz-21** to **biz-21⁻** state is accompanied by the appearance of absorption bands at 600, 850, and 960 nm. The singly reduced form showed a band at ca. 5,650 cm⁻¹, while this band is not present in the neutral form of **biz-21**.

5 Sensors

[Re(CO)$_3$(5-COOH-bpy)Cl] was found to have potential use as a pH sensor. It is weakly emissive in its protonated form, while it undergoes a 10-fold luminescence increase in its deprotonated form with a pK_a value of 5.39 [117, 144]. A sol–gel-based luminescence pH sensor capable of responding over a wide range of pH 2.3–12 based on the hydrolysis product of [Re(py–pzH)(CO)$_3$(pmat)]⁺, where py–pzH = 3-(pyridine-2-yl)pyrazole; pmat = 3-N-(pyridine-4-methylene) (aminopropyltriethoxysilane) (see Fig. 13a), has been reported. The pH-dependence was related to the protonation/deprotonation of the 3-(pyridine-2-yl)pyrazole ligand. The excited state pK_a* for [Re(py–pzH)(CO)$_3$(py)]⁺ is 7.05 [145]. The acid–base behavior of both monometallic [Re(bpy)(CO)$_3$(pca)]⁺ and bimetallic [Re(bpy) (CO)$_3$(pca)Re(bpy)(CO)$_3$]²⁺, pca = 4-pyridinecarboxaldehydeazine, complexes (see Fig. 13a) was opposite to the above examples. Emission increased in the presence of H⁺ and was attributed to protonation of one of the N atoms of the –C=N–N=C– group of the pca ligand. The excited state pK_a* value for this complex is 2.7 [146].

Beer et al. reported the use of a modified 2,2′-bipyridine ligand bonded to {Re(CO)$_3$Cl} (see Fig. 13b) as the anion sensor [147]. The modified bipyridine ligand contained a macrocyclic NH-cavity capped with a calix[4]arene strapped on its back. An increase in emission was found upon addition of Cl⁻, OAc⁻, H$_3$PO$_4$⁻ with a preference for OAc⁻.

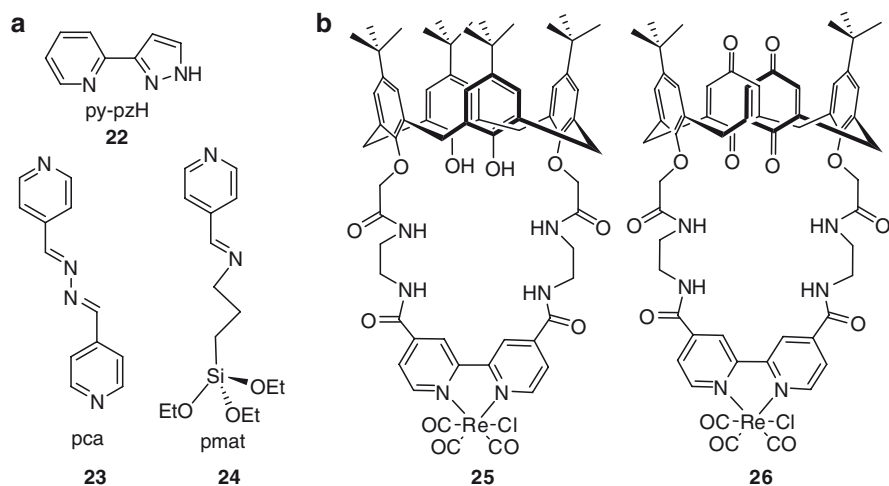**Fig. 13** (**a**) pH sensor ligands and (**b**) calix[4]arene{Re(CO)$_3$Cl}complexes

In a simpler approach, Lees' group reported that rhenium-bpy complexes of the type **27** (see Fig. 14) containing amide-type receptors served as anion binding sites [28, 148]. In this case, emission intensity was quenched in the presence of several anions: CN^-, F^-, Cl^-, Br^-, I^-, OAc^-, $H_2PO_4^-$, NO_3^-, and ClO_4^-. The complex showed strong binding affinity toward halides, cyanide, or acetate anions, while only moderate binding affinity toward dihydrogen phosphate and very weak binding affinity to nitrate or perchlorate anions. The overall order determined for binding affinity is: $CN^- > F^- > I^- > Cl^- \sim Br^- \sim OAc^- \gg H_2PO_4^- > NO_3^- > ClO_4^-$. In fact, a combination of interactions such as electrostatic, hydrogen bonding, and steric effects, apparently influence the binding affinities toward anions in this complex. The red shift of the emission band, however, indicates that the emission quenching is associated with a change in the energy of the excited state and, thus, an enhancement of nonradiative decay. The sensitivity for CN^- and F^- was so high that quenching of 10% was observed at 10^{-8} M ion concentration.

Fletcher et al. reported another interesting neutral dinuclear rhenium complex **28** (see Fig. 15) which interacts strongly with $H_2PO_4^-$, reasonably with Cl^- but only
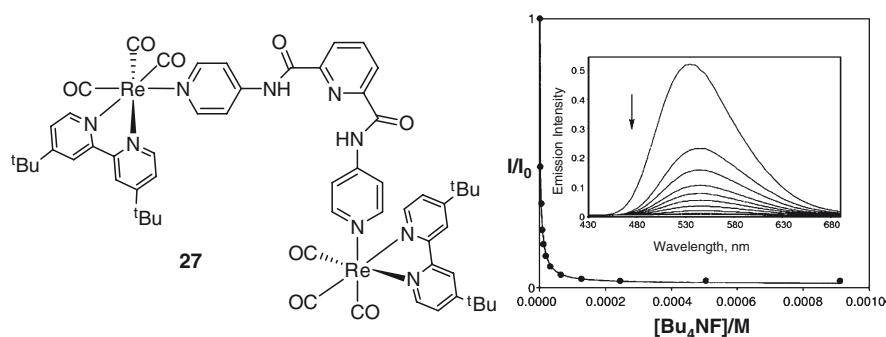

Fig. 14 The molecular structure of complex **27** and a titration plot with the addition of $[^nBu_4N]F$ ion (*right*). *Inset* shows the change in emission intensity of **27** in CH_2Cl_2 on addition of F^- ion (reproduced with permission from [28])
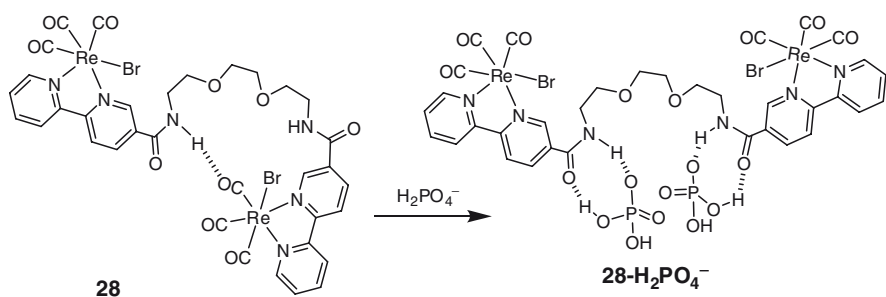

Fig. 15 Proposed mechanism for conformational change upon introduction of $[^nBu_4N]H_2PO_4$ to complex **28**

weakly with Br^-, HSO_4^-, and NO_3^-. Here, the recognition is driven by internal hydrogen bonding between the complex and the added anion [149]. The complex shows very strong affinity for dihydrogenphosphate over chloride (for $H_2PO_4^-$, β_2 = 3.5 × 10^5 M^{-1}; for Cl^-, β_2 = 1.5 × 10^4 M^{-1}). Addition of the $H_2PO_4^-$ anion to the complex gave rise to a large increase in the emission at 632 nm and a concomitant blue shift of 10 nm, related to the energy increase of the MLCT state. The increase in emission was due to the unfolding of the structure as hydrogen bonds are broken between the amide and rhenium carbonyl.

Cation recognition by luminescent rhenium carbonyl diimine complexes has also been reported. Moore and coworkers reported release and recapture of alkali and alkaline earth metal ions for $[Re(CO)_3(bpy)L_4]^+$ (vide supra) [46]. Yam et al. reported a series of interesting rhenium(I) tricarbonyl phenanthroline complexes with crown ether pendants (see Fig. 16) [150]. These complexes showed selective and specific binding properties for various metal cations of different sizes and degrees of hardness and softness by variation of the cavity size and donor atoms of the crown ether. A strong enhancement in the emission intensity was observed upon binding of the metal ions to the complexes. Such an enhancement in the emission intensity is due to blocking of the intramolecular reductive electron-transfer quenching mechanism, since the coordination of metal ions into the crown cavity reduces the ability of the donor atoms in the crown unit to quench the emissive ^{3}MLCT state by photoinduced electron transfer. The slight red shift of the emission maxima was explained by the fact that binding of the cation to the crown would decrease the σ-donating ability and stabilize the π* orbital of the phenanthroline ligand and, hence, decrease the emission intensity.

Lo et al. synthesized a number of luminescent rhenium(I) diimine-biotin complexes of the type, $[Re(N-N)(CO)_3(py-biotin)]^+$, where N–N is 1,10-phenanthroline (or derivative) and py-biotin is a pyridyl ligand attached with biotin containing different spacer-arms (see Fig. 17) [151–153]. The complexes show intense high-energy absorption at ca. 248–300 nm that are assigned to spin-allowed ^{1}IL (π→π*) (diimine and py-biotin ligands), while the less intense absorption shoulders at ca. 320–400 nm are assigned to spin-allowed dπ(Re)→π*(diimine) ^{1}MLCT transitions. Upon photoexcitation, each of these complexes exhibited intense and long-lived dπ(Re)→π*(diimine) ^{3}MLCT luminescence in solution at ambient temperature. These complexes show a very large Stokes shift of ca. 7,657 cm^{-1}. The most remarkable observation was that the biotin-incorporated rhenium complexes dis-
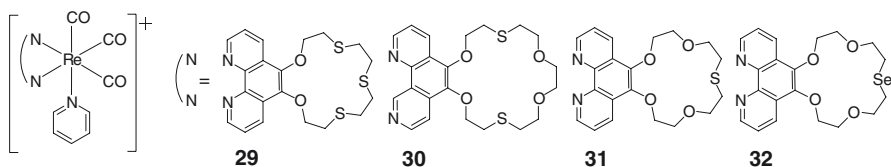

Fig. 16 Rhenium(I) tricarbonyl diimine complexes with crown ether pendants as metal cation sensors
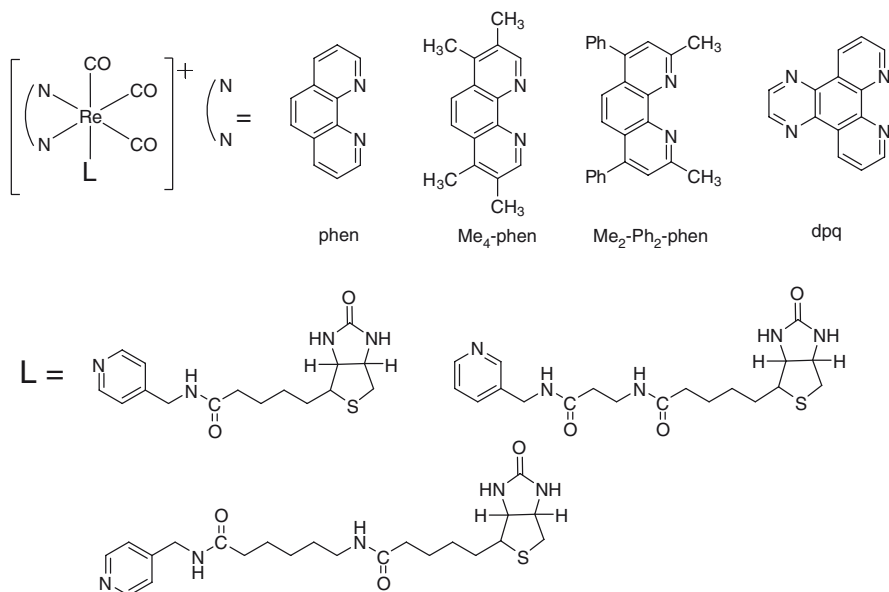
Fig. 17 Luminescent rhenium(I) tricarbonyl diimine-biotin complexes as probes for avidin

play enhanced emission intensities and extended lifetimes upon binding to avidin. Since no similar changes were observed when excess biotin was present, the increase in emission intensities and lifetimes was attributed to a specific binding of the complexes to the biotin-binding site of avidin. These observations are in contrast to most fluorophore–biotin conjugates, which suffer from severe emission quenching upon binding to avidin due to resonance-energy transfer (RET), unless exceptionally long spacers such as poly(ethylene glycol) are present between the fluorophore and biotin unit [154]. The absence of emission quenching in rhenium(I)-biotin complexes is because of the insignificant overlap between their absorption and emission spectra, which disfavors RET quenching.

The enhancement of the emission intensities and lifetimes can be further explained by considering the hydrophobicity associated with the binding pockets of avidin, as the lifetimes of these complexes are sensitive to the hydrophobicity of the environment. Another reason for the enhancement of emission and lifetime is the increased rigidity of the surroundings of the complexes upon binding to avidin, which may lead to lower nonradiative decay, thereby more intense and longer-lived emission. Hence, rhenium(I) polypyridine–biotin complexes offer remarkable advantages over traditional biotin–fluorophores as probes for avidin and can be utilized in homogeneous assays for biotin and biotinylated biomolecules.

Sun's group reported the synthesis, characterization, and photophysical properties of a series of organic receptors and their corresponding Re(I) tricarbonyl complexes as anion probes, featuring bis-sulfonamide as interacting sites attached to highly chromophoric π-conjugated quinoxaline moieties (see Fig. 18) [155].
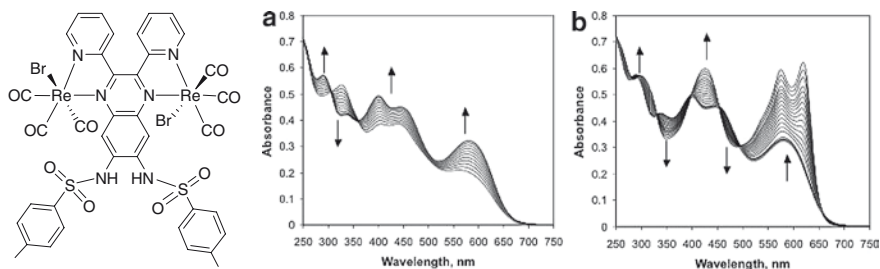
Fig. 18 The structure of rhenium(I) tricarbonyl diimine complex for anion sensing and the absorption spectral changes of this probe molecule (2.5×10^{-5} M) in CH$_3$CN upon addition of n-Bu$_4$NF, (**a**) [F$^-$] = 0 – 2.8×10^{-5} M and (**b**) [F$^-$] = 2.8×10^{-5} – 1.1×10^{-4} M. (reproduced with permission from [155])

The interactions with various anions were extensively investigated. These probe molecules are capable of recognizing F$^-$, OAc$^-$, CN$^-$, and H$_2$PO$_4^-$ with different sensitivity. The probe-anion interactions can be easily visualized by naked eye colorimetric responses. Moreover, the anion-probe interaction can also be monitored by the metal carbonyl stretching frequencies. The colorimetric responses upon addition of anions were attributed to the direct N-H deprotonation of sulfonamide groups.

6 Light-Emitting Devices

Figure 19 shows the rhenium(I) diimine complexes exploited as dopants in *organic light-emitting diodes* (OLEDs) [46–52]. The trifunctional molecule **33** was synthesized integrating three functions needed for efficient operation of OLEDs. The molecule contains an emissive chromophore (a Re^I polypyridyl complex containing dipyrido[3,2-a-2′,3′-c]phenazine), an electron-transporting 1,3,4-oxadiazole group, and a hole-transporting terthiophene unit. The HOMO and LUMO energies of the complex lie within the band gap of the host polymer, poly(*N*-vinylcarbazole) (PVK), a property suggesting its potential use as an OLED [46]. Electrically neutral rhenium(I) tricarbonyl complexes **34–38** were used as emitters for electrophosphorescent devices. Complex **34** was used as an orange-emitting dopant in a 4, 4′-*N*, *N*′-dicarbazole-biphenyl host to fabricate *phosphorescent organic light-emitting diodes* (PhOLEDs). The maximum electroluminescence (EL) efficiency and luminescence of 21.8 cd A^{-1}, and 8,315 cd cm^{-2} at 17.5 V were obtained, respectively, and so far this is the best electroluminescence reported for Re^I-doped PhOLEDs [47]. The improvement in electroluminescent performance could be attributed to the synergistic effects of the two reciprocally repulsive phenyl and methyl groups in the backbone of the 1,10-phenanthroline molecule.
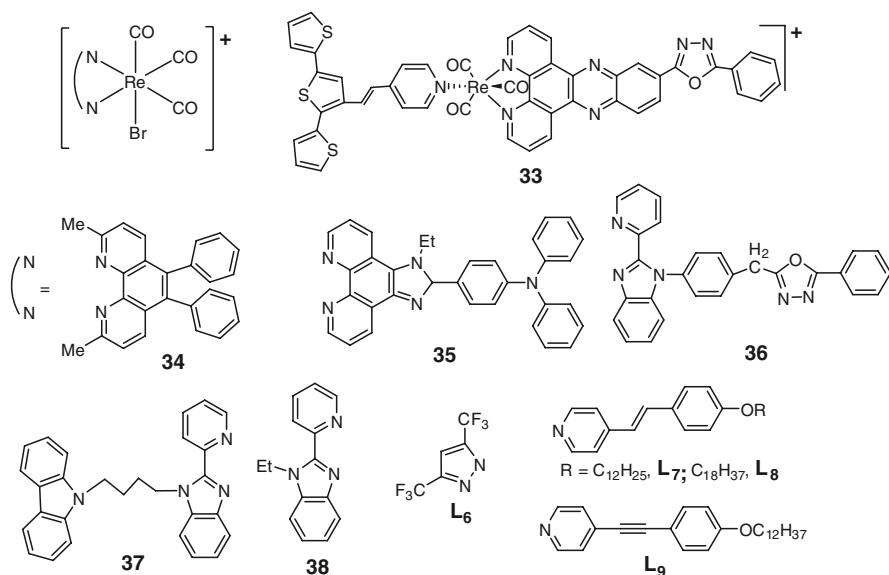
Fig. 19 Rhenium(I) tricarbonyl diimine complexes for LEDs

The OLED devices incorporating complex **35** functionalized by triphenylamine, a hole transport group, emit strong yellow–green light with an emission maximum at 552 nm [48]. A current efficiency up to 17.6 cd A^{-1} corresponding to a power efficiency of 9.2 Im W^{-1} at 6 V and peak brightness as high as 6,500 cd m^{-2} at 16 V were achieved. Complex **36** showed a maximum brightness of 1,174 cd m^{-2} at 17 V, while the devices based on the carbazole-containing (hole transport group) complex **37** showed a maximum brightness of 2,300 cd m^{-2} at 16 V [49]. The devices with a doping concentration of 10 wt% of **36** and **37** showed a maximum efficiency at 230 mA cm^{-2} and still possessed 51% of the maximum efficiency at 4.2 mA cm^{-2} for 36 and 56% of the maximum efficiency at 2.7 mA cm^{-2} for 37, respectively. A two-layer electroluminescent device of a rhenium(I) tricarbonyl complex of 2-(1-ethylbenzimidzol-2-yl)pyridine **38** with a configuration of ITO/TDP/**38**/Mg$_{0.9}$Ag$_{0.9}$/Ag gave a turn-on voltage as low as 3 V and a maximum luminescence of 113 cd m^{-2} at a bias voltage of 10.5 V [156].

The complexes [Re(bpy)(CO)$_3$(**L$_6$**)]$^+$ and [Re(phen)(CO)$_3$(**L$_6$**)]$^+$ were used as dopants in host materials 4,4′-dicarbazolylbiphenyl (CBP) and 2,2′,2″-(1,3,5-benzenetriyl)-tris[1-phenyl-1H-benzimidazole] (TBPI) and sublimable in the temperature range 150–165ºC in vacuum [50]. For [Re(bpy)(CO)$_3$(**L$_6$**)]$^+$, electrophosphorescence occurred at 530 nm at a turn-on voltage of 6 V with a luminescence power of 0.72 Im W^{-1} and luminescence of 2,300 cd m^{-2} at a current density of 100 mA cm^{-2}. Rhenium(I) 2,2′-bipyridine surfactant complexes [Re(bpy)(CO)$_3$(**L$_{7,8,9}$**)]PF$_6$ formed stable Langmuir-Blodgett films that served as the emitting layer in OLEDs. An OLED consisting of 25 layers with ITO glass at the bottom and Al on top took 7 V to turn-on and 18 V to reach 9 cd cm^{-2} [157].

Rhenium(I) tricarbonyl-2,2′-bipyridine moieties were used to cap both ends of a poly fluorine, yielding Re-capped $\{Re(bpy)(CO)_3(py)-X-(py)(CO)_3(bpy)Re\}^{2+}$ polymers, where X = polyfluorene [51, 52]. The polymers with and without the Re caps were spin-coated from their solutions in CH_2Cl_2 onto an ITO surface previously modified with a layer of poly(styrene sulfonic acid), doped with poly(ethylenedioxythiophene). The LED (light-emitting device) was then topped with a layer of Ca/Al. The photoluminescence (PL) and electroluminescence seen were consistent with the presence of $[Re(bpy)(CO)_3(py)]^+$ [158].

References

1. Holten D, Bocian DF, Lindsey JS (2002) Acc Chem Res 35:57
2. Remacle F, Levine RD (2001) J Phys Chem B 105:2153
3. Yeow EKL, Steer RP (2003) Phys Chem Chem Phys 5:97
4. Yeow EKL, Steer RP (2003) Chem Phys Lett 377:391
5. Geoffroy GL, Wrighton MS (1979) Organometallic photochemistry. Academic, New York
6. Wrighton M, Morse DL (1974) J Am Chem Soc 96:998
7. Lees AJ (1987) Chem Rev 87:711
8. Lees AJ, Sun SS in McCleverty JA, Meyer TJ (Eds) (2004) Comprehensive coordination chemistry II, Vol 2. Elsevier, Oxford, UK, p 731
9. Kirgan RA, Sullivan BP, Rillema DP in Balzani V, Campagna S (Eds) (2007) Top Curr Chem 281:45
10. Lees AJ (1995) Comments Inorg Chem 17:319
11. Chen P, Meyer TJ (1998) Chem Rev 98:1439
12. Stufkens DJ (1992) Comments Inorg Chem 13:359
13. Vogler A, Kunkely H (2000) Coord Chem Rev 200–202:991
14. Balzani V, Juris A, Venturi M, Campagna S, Serroni S (1996) Chem Rev 96:759
15. Schanze KS, Walters KA (2000) Photoinduced electron transfer in metal-organic dyads. In: Ramamurthy V, Schanze KS (Eds) Organic and Inorganic Photochemistry. Molecular and Supramolecular Photochemistry Series, Vol 2, Chap 3. Marcel Dekker, New York, p 75
16. Schanze KS, MacQueen DB, Perkins TA, Cabana LA (1993) Coord Chem Rev 122:63
17. Worl LA, Duesing R, Chen P, Della Ciana L, Meyer TJ (1991) J Chem Soc Dalton Trans:849
18. Stufkens DJ, Vlček A Jr (1998) Coord Chem Rev 177:127
19. Kalyanasundaram K (1992) Photochemistry of polypyridine and porphyrin complexes, Chap 10. Academic, New York, p 321
20. Caspar JV, Meyer TJ (1983) J Phys Chem 87:952
21. Takeda H, Koike K, Inoue H, Ishitani O (2008) J Am Chem Soc 130:2023
22. Abdel-Shafi AA, Bourdelande JL, Ali SS (2007) Dalton Trans:2510
23. Belliston-Bittner W, Dunn AR, Nguyen YHL, Stuehr DJ, Winkler JR, Gray HB (2005) J Am Chem Soc 127:15907
24. Hayashi Y, Kita S, Brunschwig BS, Fujita E (2003) J Am Chem Soc 125:11976
25. Hwang J-S, Chang J-S, Park S-F, Ikeue K, Anpo M (2005) Top Cat 35:311
26. Kumar A, Sun SS, Lees AJ (2008) Coord Chem Rev 252:922
27. Sun SS, Less AJ (2002) Coord Chem Rev 230:171
28. Sun SS, Lees AJ (2000) Chem Commun:1687
29. Mizuno T, Fukumatsu T, Takeuchi M, Shinkai S (2000) J Chem Soc Perkin Trans 1:407
30. Keefe MH, Sloan RV, Hupp JT, Czaplewski KF, Snurr RQ, Stern CL (2000) Langmuir 16:3964
31. Bakir M, McKenzie JAM (1997) J Chem Soc Dalton Trans:3571

32. De Silva AP, Gunaratne HQN, Gunnlaugsson T, Huxley AJM, McCoy CP, Rademacher JT, Rice TE (1997) Chem Rev 97:1515
33. Demas JN, DeGraff BA (1991) Anal Chem 63:A829
34. Lees AJ (1998) Coord Chem Rev 177:3
35. Lees AJ (2001) Luminescent metal complexes as spectroscopic probes of monomer/polymer environments. In: Ramamurthy V, Schanze KS (Eds) Optical Sensors and Switches. Molecular and Supramolecular Photochemistry Series, Vol 7, Chap 5. Marcel Dekker, New York, p 209
36. Sun SS, Lees AJ (2002) Organometallics 21:39
37. Polo AS, Itokazu MK, Frin KM, Patrocnio AOT, Iha NYM (2006) Coord Chem Rev 250:1669
38. Argazzi R, Bertolasi E, Chiorboli C, Bignozzi CA, Itokazu MK, Iha NYM (2001) Inorg Chem 40:6885
39. Lewis JD, Perutz RN, Moore JN (2000) J Chem Soc Chem Commun:1865
40. Sun SS, Robson E, Dunwoody N, Silva AS, Brinn IM, Lees AJ (2000) J Chem Soc Chem Commun:201
41. Fernandez-Acebes A, Lehn JM (1999) Chem Eur J 5:3285
42. Yam VWW, Lau VCY, Wu LX (1998) J Chem Soc Dalton Trans:1461
43. Schanze KS, Lucia LA, Cooper M, Walters KA, Ji HF, Sabina O (1998) J Phys Chem A 102:5577
44. Beyeler A, Belser P, De Cola L (1997) Angew Chem Int Ed Engl 36:2779
45. Yam VWW, Lau VCY, Cheung KK (1995) J Chem Soc Chem Commun:259
46. Lundin NJ, Blackman AG, Gordon KC, Officer DL (2006) Angew Chem Int Ed 45:2582
47. Li X Zhang D, Li W, Chu B, Han l, Zhu J, Su Z, Bi D, Wang D, Yang D, Chen Y (2008) Appl Phys Lett 92:083302
48. Liu C, Li J, Li B, Hong Z, Zhao F, Liu S, Li W (2006) Appl Phys Lett 89:243511
49. Si z, Li J, Li B, Zhao F, Liu S, Li W (2007) Inorg Chem 46:6155
50. Ranjan S, Lin S-Y, Hwang K-C, Chi Y, Ching W-L, Liu C-S (2003)Inorg Chem 42:1248
51. Zhang Y, Huang z, Zeng W, Cao Y (2008) Polymer 49:1211
52. Lee P-I, Hsu SL-C, Chung C-T (2006) Synth Metals 156:907
53. Zhang J, Chu BW-K, Zhu N, Yam VW-W (2007) Organometallics 26:5423
54. Yam VWW, Yang Y, Yang HP, Cheung KK (1999) Organometallics 18:5252
55. Briel O, Sunkel K, Krossing I, Noth H, Schmalzlin E, Meerholz K, Brauchle C, Beck W (1999) Eur J Inorg Chem:483
56. Bourgault M, Baum K, Le Bozec H, Pucetti G, Ledoux I, Zyss J (1998) New J Chem:517
57. Victor RF, Correia I, Videira M, Marques F, Paulo A, Pessoa JC, Viola G, Martins GG, Santos I (2008)Chem Bio Chem 9:131
58. Ma D-L, Che C-M, Siu F-M, Yang M, Wong K-Y (2007) Inorg Chem 46:740
59. Ruiz GT, Juliarena MP, Lezna RO, Wolcan E, Feliz MR, Ferraudi G (2007) J Chem Soc Dalton Trans:2020
60. Reece SY, Nocera DG (2005) J Am Chem Soc 127:9448
61. Stoeffler HD, Thornton NB, Temkin SL, Schanze KS (1995) J Am Chem Soc 117:7119
62. Fuks L, Gniazdowska E, Meiczkowski J, Sadlej-Sosnowska N (2008) Polyhedron 27:1353
63. Tzanopoulou S, Pirmettis IC, Patsis G, Paaravatou-Petsotas M, Livaniou E, Papadopoulos M, Pelecanou M (2006) J Med Chem 49:5408
64. Dunn AR, Belliston-Bittner W, Winkler JR, Getzoff ED, Stuehr DJ, Gray HB (2005) J Am Chem Soc 127:5169
65. Zhang J, Vittal JJ, Henderson W, Wheaton JR, Hall IH, Hor TSA, Yan YK (2002) J Organomet Chem 650:123
66. Pietzsch H-J, Gupta A, Reisgys M, Drews A, Seifert S, Syhre R, Spies H, Alberto R, Abram U, Schubiger PA, Johannsen B (2000) Bioconjugate Chem 11:414
67. Stoyanov SR, Villegas JM, Cruz AJ, Lockyear LL, Reibenspies JH, Rillema DP (2005) J Chem Theory Comput 1:95
68. Villegas JM, Stoyanov SR, Huang W, Rillema DP (2005) Inorg Chem 44:2297
69. Villegas JM, Stoyanov SR, Huang W, Rillema DP (2005) Dalton Trans:1042

70. Gabrielsson A, Busby M, Matousek P, Towrie M, Hevia E, Cuesta L, Perez J, Zális S, Vlček A Jr (2006) Inorg Chem 45:9789
71. Kirgen R, Simpson M, Moore C, Day J, Bui L, Tanner C, Rillema DP (2007) Inorg Chem 46:6464
72. Zhao G-J, Zhou X, Liu T, Zheng Q-C, Bai F-Q, Zhang H-X (2008) J Mol Struct Theochem 855:52
73. Machura B, Kruszynski R (2007) J Organomet Chem 692:4161
74. Baiano JA, Kessler RJ, Lumpkin RS, Munley MJ, Murphy WR Jr (1995) J Phys Chem 99:17680
75. Hino JK, Della Ciana L, Dressick WJ, Sullivan BP (1992) Inorg Chem 31:1072
76. Kalyanasundaram K (1986) J Chem Soc Faraday Trans 2 82:2401
77. Schoonover JR, Strouse GF (1998) Chem Rev 98:1335
78. Schoonover JR, Bignozzi CA, Meyer TJ (1997) Coord Chem Rev 165:239
79. Schoonover JR, Strouse GF, Dyer RB, Bates WD, Chen P, Meyer TJ (1996) Inorg Chem 35:273
80. George MW, Johnson FPA, Westwell JR, Hodges PM, Turner JJ (1993) J Chem Soc Dalton Trans:2977
81. Walters KA, Dattelbaum DM, Ley KD, Schoonover JR, Meyer TJ, Schanze KS (2001) J Chem Soc Chem Commun:1834
82. Schoonover JR, Chen P, Bates WD, Dyer RB, Meyer TJ (1994) Inorg Chem 33:793
83. Chen P, Curry M, Meyer TJ (1989) Inorg Chem 28:2271
84. Shaver RJ, Perkovic MW, Rillema DP, Woods C (1995) Inorg Chem 34:5446
85. Katz NE, Mecklenburg SL, Graff DK, Chen P, Meyer TJ (1994) J Phys Chem 98:8959
86. Chen P, Westmoreland TD, Danielson E, Schanze KS, Anthon D, Neveux PE Jr, Meyer TJ (1987) Inorg Chem 26:1116
87. Chen P, Duesing R, Graff DK, Meyer TJ (1991) J Phys Chem 95:5850
88. Schoonover JR, Strouse GF, Chen P, Bates WD, Meyer TJ (1993) Inorg Chem 32:2618
89. Vlček A Jr , Busby M (2006) Coord Chem Rev 250:1755
90. Wang Y, Schanze KS (1996) J Phys Chem 100:5408
91. Trammell S, Goodson PA, Sullivan BP (1996) Inorg Chem 35:1421
92. Wang Y, Lucia LA, Schanze KS (1995) J Phys Chem 99:1961
93. Lucia LA, Wang Y, Nafisi K, Netzel TL, Schanze KS (1995) J Phys Chem 99:11801
94. Wang Y, Schanze KS (1993) Chem Phys 176:305
95. Wang Y, Hauser BT, Rooney MM, Burton RD, Schanze KS (1993) J Am Chem Soc 115:5675
96. Rossenaar BD, Stufkens DJ, Vlcek A Jr (1996) Inorg Chem 35:2902
97. Giordano PJ, Fredericks SM, Wrighton MS, Morse DL (1978) J Am Chem Soc 100:2257
98. Wallace L, Rillema DP (1993) Inorg Chem 32:3836
99. Wallace L, Jackman DC, Rillema DP, Merkert JW (1995) Inorg Chem 34:5210
100. Leasure RM, Sacksteder L, Nesselrodt D, Reitz GA, Demas JN, DeGraff BA (1991) Inorg Chem 30:3722
101. Del Guerzo AD, Leroy S, Fages F, Schmehl RH (2002) Inorg Chem 41:359
102. Ziessel R, Juris A, Venturi M (1998) Inorg Chem 37:5061
103. Baba AI, Shaw JR, Simon JA, Thummel RP, Schmehl RH (1998) Coord Chem Rev 171:43
104. Schoonover JR, Bates WD, Meyer TJ (1995) Inorg Chem 34:6421
105. Vlcek A Jr (1998) Coord Chem Rev 177:219
106. Koike K, Okoshi N, Hori H, Takeuchi K, Ishitani O, Clark IP, George MW, Johnson FPA, Turner JJ (2002) J Am Chem Soc 124:11448
107. Koike K, Tanabe J, Toyama S, Tsubaki H, Sakamoto K, Westwell JR, Johnson FPA, Hori H, Saitoh H, Ishitani O (2000) Inorg Chem 39:2777
108. Hightower SE, Corcoran RC, Sullivan BP (2005) Inorg Chem 44:9601
109. Sato S, Sekine A, Ohashi Y, Ishitani O, Blanco-Rodriguez AM, Vlček A Jr, Unno T, Koike K (2007) Inorg Chem 46:3531
110. Del Negro AS, Woessner SM, Sullivan BP, Dattelbaum DM, Schoonover JR (2001) Inorg Chem 40:5056

111. Rossenaar BD, Kleverlaan CJ, Stifkens DJ, Sskam A (1994) J Chem Soc Chem Commun:63
112. Gabrielsson A, Blanco-Rodríguez AM, Matousek P, Towrie M, Vlček A Jr (2006) Organo-metallics 25:2148
113. Wenger OS, Henling LM, Day MW, Winkler JR, Gray HB (2004) Inorg Chem 43:2043
114. Yam VW-W, Yang Y, Zhang J, Chu BW-K, Zhu N (2001) Organometallics 20:4911
115. Busby M, Matousek P, Towrie M, Vlček A Jr (2007) Inorganica Chimica Acta 360:885
116. Lewis JD, Perutz RN, Moore JN (2004) J Phys Chem A 108:9037
117. Yam VW-W, Ko C-C, Wu L-X, Wong KM-C, Cheung K-K (2000) Organometallics 19:1820
118. Ko C-C, Wu L-X, Wong KM-C, Zhu N, Yam VW-W (2004) Chem Eur J 10:766
119. Lee PH-M, Ko C-C, Zhu N, Yam VW-W, (2007) J Am Chem Soc 129:6058
120. Ko C-C, Kwok W-M, Yam VW-W, Phillips DL (2006) Chem Eur J 12:5840
121. Yam VW-W, Ko C-C, Zhu N (2004) J Am Chem Soc 126:12734
122. Manimaran B, Thanasekaren P, Rajendran T, Lin R-J, Chang I-J,Lee G-H, Peng S-M, Rajagopal S, Lu K-L (2002) Inorg Chem 41:5323
123. Woessner SM, Helms JB, Shen Y, Sullivan BP (1998) Inorg Chem 37:5406
124. Thanasekaren P, Liao R-T, Manimaran B, Liu Y-H, Chou P-T, Rajagopal S, Lu K-L (2006) J Phys Chem A 110:10683
125. Rajendran T, Manimaran B, Liao R-T, Lin R-J, Thanasekaran P, Lee G-H, Peng S-M, Liu Y-H, Chang I-J, Rajgopal S, Lu K-L (2003) Inorg Chem 42:6388
126. Sun S-S, Lees AJ (2000) J Am Chem Soc 122:8956
127. Sun S-S, Lees AJ (1999) Inorg Chem 38:4181
128. Slone RV, Hupp JT, Stern CL, Albrecht-Schmitt TE (1996) Inorg Chem 35:4096
129. Lee SJ, Lin W, (2002) J Am Chem Soc 124:4554
130. Benkstein KD, Hupp JT, Stern CL (1998) J Am Chem Soc 120:12982
131. Vogler A, Kisslinger J (1986) Inorg Chim Acta 115:193
132. Benkstein KD, Hupp JT, Stern CL (2002) Angew Chemie Int Ed Eng 39:2891
133. Benkstein KD, Stern CL, Splan KE, Johnson RC, Walters KA, Vanhelmont FWM, Hupp JT (2002)Eur J Inorg Chem :2818
134. Slone RV, Yoon DI, Calhoun RM, Hupp JT (1995) J Am Chem Soc 117:11813
135. Sun S-S, Anspach JA, Lees AJ (2002) Inorg Chem 41:1862
136. Sathiyendiran M, Liao R-T, Thanasekaran P, Luo T-T, Venkataramanan NS, Lee G-H, Peng S-M, Lu K-L (2006) Inorg Chem 45:10052
137. Slone RV, Hupp JT (1997) Inorg Chem 36:5422
138. Sun S-S, Lees AJ (2001) Inorg Chem 40:3154
139. Splan KE, Massari AM, Morris GA, Sun S-S, Reina E, Nguyen ST, Hupp JT (2003) Eur J Inorg Chem :2348
140. Kumar A, Sun S-S, Lees AJ (2008) Coord Chem Rev 252:922
141. de Wolf P, Heath S, Thomas J (2002) J Chem Soc Chem Commun:2540
142. Sun S-S, Lees AJ (2001) Chem Commun:103
143. Manimaran B, Rajendran T, Lu Y-L, Lee G-H, Peng S-M, Lu K-L (2001) Eur J Inorg Chem:633
144. Amendola V, Bacchilega D, Costa I, Gianelli L, Montalti M, Pallavicini P, Perotti A, Prodi L, Zaccheroni N (2003) J Photochem Photobiol A: Chem 159:249
145. Lam MHW, Lee DYK, Man KW, Lau CSW (2000) J Mater Chem 10:1825
146. Cattaneo M, Fagalde F, Katz NE (2006) Inorg Chem 45:6884
147. Beer PD, Timoshenko V, Maestri M, Passaniti P, Balzani V (1999) J Chem Soc Chem Commun:1755
148. Sun S-S, Lees AJ, Zavalij PY (2003) Inorg Chem 42:3445
149. Pelleteret D, Fletcher NC, Doherty AP (2007) Inorg Chem 46:4386
150. Li, M-J, Ko C-C, Duan G-P, Zhu N, Yam VW-W (2007) Organometallics 26:6091
151. Lo KK-W, Hui W-K (2005) Inorg Chem 44:1992
152. Lo KK-W, Hui W-K (2002) J Am Chem Soc 124:9344

153. Lo KK-W, Hui W-K, Chung C-K, Tsang KH-K, Lee TK-M, Li C-K, Lau JS-Y, Ng DC-M (2006) Coord Chem Rev 250:1724
154. Grubber, HJ Kada HG, Riener CK, Harms GS, Ahrer W, Dax TG, Knaus HG, (2000) Bioconjugate Chem 11:696
155. Lin T-P, Chen C-Y, Wen Y-S, Sun S-S (2007) Inorg Chem 46:9201
156. Wang K, Huang L, Gao L, Jin L, Huang C (2002) Inorg Chem 41:3353
157. Yam VW-W, Li B, Yang Y, Chu BW-K, Wong KM-C, Cheung K-K (2003) Eur J Inorg Chem:4035
158. Dinolfo, PH Coropceanu V, Bredas J-L, Hupp JT, (2006) J Am Chem Soc 128:12592